Tribology Letters (2025) 73:18
https://doi.org/10.1007/s11249-024-01933-6

ORIGINAL PAPER

On How to Determine Surface Roughness Power Spectra

N. Rodriguez[1,2] · L. Gontard[3] · C. Ma[4] · R. Xu[4,5,6] · B. N. J. Persson[4,5,6]

Received: 16 July 2024 / Accepted: 28 October 2024

Abstract

Analytical contact mechanics theories depend on surface roughness through the surface roughness power spectrum. In the present study, we evaluated the usability of various experimental methods for studying surface roughness. Our findings indicated that height data obtained from optical methods often lack accuracy and should not be utilized for calculating surface roughness power spectra. Conversely, engineering stylus instruments and atomic force microscopy (AFM) typically yield reliable results that are consistent across the overlapping roughness length scale region. For surfaces with isotropic roughness, the two-dimensional (2D) power spectrum can be derived from the one-dimensional (1D) power spectrum using several approaches, which we explored in this paper.

Graphical Abstract

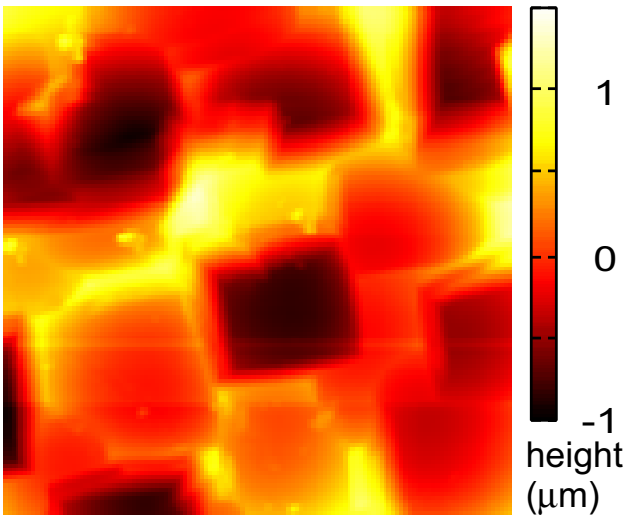

Keywords Surface roughness · Engineering stylus · Atomic force microscopy · Power spectrum · Height topography

✉ B. N. J. Persson
b.persson@fz-juelich.de

[1] BD Medical-Pharmaceutical Systems 1 Becton Drive, Franklin Lakes, NJ 07419, USA

[2] Orlando Christian Prep, 500 S Semoran Blvd., Orlando, FL 32807, USA

[3] BD Medical-Pharmaceutical Systems, 11 Rue Aritides-Verges, 38801 Le Pont de Claix, France

[4] Peter Grünberg Institute (PGI-1), Forschungszentrum Jülich, Jülich 52425, Germany

[5] State Key Laboratory of Solid Lubrication, Lanzhou Institute of Chemical Physics, Chinese Academy of Sciences, Lanzhou 730000, China

[6] Multiscale Consulting, Wolfshovener Str. 2, Jülich 52428, Germany

Published online: 27 December 2024

1 Introduction

The quality of the surfaces of solids has become extremely important in the design and production of components in particular in high tech applications [1–5] and biological and medical applications [6–10]. This is particularly true for the microgeometry (surface roughness). In most engineering applications just one or two parameters (numbers) are given to characterize the surface roughness. The most common parameters are the arithmetical average Ra and the maximum height parameter Rz, both of which can be obtained from a single line scan of the height topography. Some studies also present the height probability distribution P_h and the surface roughness power spectrum $C(\mathbf{q})$, from which most standard surface roughness parameters can be obtained [11–16].

Randomly rough surfaces are surfaces that can be represented as a sum of plane waves with random phases. For such surfaces, the power spectra contain all the (ensemble averaged) information about the surface roughness. For this reason in most analytical contact mechanics theories (with or without adhesion) the roughness enters only as $C(\mathbf{q})$. In these theories, the (ensemble averaged) area of real contact, the interfacial stress distribution, and the distribution of interfacial separations are all determined by $C(\mathbf{q})$ [17–19].

Fundamental investigations about surface roughness were performed by Longuet-Higgins, who analyzed the statistical geometry of random surfaces [20], and also a general statistical analysis of a random, moving surface [21]. Nayak introduced a random process model of rough surfaces, and studied the properties of height-height correlation functions in both real and wavevector space [11]. The properties of random rough surfaces of significance in their contact was studied by Whitehouse and Archard [22], and Gray and Johnson studied the dynamic response of elastic bodies in rolling contact with random roughness of their surfaces [23].

All topography measurements involve interaction between the sensing probe and the surface. Some methods involve a direct (probe-tip–substrate) solid contact while others involve exposing the studied solid to electromagnetic waves or electron beams, which may modify the surface topography. For solid contact methods like stylus, the contact stress at the probe tip may be very high resulting in elastoplastic deformation and scratches on the studied surfaces. Non-contact methods like optical (e.g., laser-based) methods may locally increase the temperature and induce thermally activated processes and surface modifications. We note that some materials, like soft gels and some biological materials, cannot be studied directly using engineering stylus instruments, and even non-contact AFM may be problematic in some cases because it exposes the substrate surfaces to attractive (e.g., Van der Waals or electric) forces and repulsive forces when the tip is close to the surface. For stylus measurements on soft solids, e.g., soft rubber materials, the attractive tip-substrate force can effectively modify the surface topography as observed for silicone rubber (PDMS) where stick-slip occurred [24]. However, sometimes replicas made using an elastically stiff (glassy) polymer can be obtained from soft (and hard) solids and the topography of the replica can be studied using stylus instruments [24]. When transparent materials are studied using optical methods several problems may occur e.g., reflections of the electromagnetic waves from the internal surfaces of the sample, as observed in some cases for ice [25]. Scanning tunneling microscopy (STM) can only be performed on materials with high enough electric conductivity and the tunneling electrons can result in surface modifications, at least on the atomic scale.

Several experimental methods have been used to obtain surface roughness power spectra:

(a) Optical methods, e.g., light scattering or interferometric methods [26].
(b) Stylus methods, e.g., engineering stylus and atomic force microscopy (AFM) [27].
(c) Optical, Xerographic, X-ray, and neutron reflectivity, or electron microscopy study of the line profile of vertical sections (thin slices) of the sample [24, 28, 29].
(d) X-Ray Tomography [30].
(e) Scanning tunneling microscopy (STM) [15, 31].

To cover all relevant length scales one usually needs to combine several methods. Optical methods are limited by the wavelength of the light and the shortest length scales that can be probed are usually of order ~ 1 μm. The (maximum) resolution of stylus measurements is determined by the radius of curvature R of the probe tip and the (minimum) curvature radius R^* of the valleys of the surface roughness profile (if $R > R^*$ the tip cannot penetrate into the cavity) [32, 33]. For engineering stylus instrument the tip curvature is typically $R \sim 1$ μm while for AFM very sharp tips with $R \sim 1$ nm are often used, and sometimes atomic structures (at nanometer length scales) can be resolved in AFM measurements. However, surface roughness at the atomic scale is a somewhat ill-defined concept and the measured topography depends on the probe-tip substrate interaction potential and charge density profiles and involves quantum mechanical considerations. However, this is really not a limitation since the atomic scale "roughness" (e.g., atomic steps or adatoms) can anyhow not be directly included in contact mechanics models (which are usually based on continuum mechanics), but require an atomistic approach such as Molecular Dynamics, so a "multi-physics" approach

may be needed to fully understand a phenomena depending on the surface roughness. Thus the shortest wavelength for which the power spectrum is needed is of order $\sim$ 1 nm.

The maximum lateral size of the studied surface area using AFM (and STM) is for most instruments of order $\sim$ 100 μm so if longer wavelength roughness matters AFM must be combined with other methods. Recently the use of optical methods has proliferated because of their simplicity and speed. These methods produce nice looking pictures but we will show that the topography is not correctly reproduced in most cases and we recommend against using optical methods for quantitative topography studies.

In this study, we will discuss the usefulness of different experimental methods on "smooth" and "rough" surfaces of elastically stiff and optically non-transparent solids. We will show how the 2D power spectra, which enter contact mechanics theories, can be obtained from the 1D power spectra. We find that in many cases optical methods fail while engineering stylus and AFM measurements usually give very good results.

2 Surface Roughness Correlation Functions

Consider a surface with the height profile $z = h(\mathbf{x})$, where $\mathbf{x} = (x, y)$ is a point in the surface plane. We assume no overhangs so that for each point $\mathbf{x}$ there is only one height coordinate $h(\mathbf{x})$. We assume that the surface is nominally flat and that we choose the origin of the z-coordinate so that $\langle h(\mathbf{x})\rangle = 0$, where $\langle ..\rangle$ stands for ensemble averaging. In the most general case, to fully characterize the statistical properties of the surface, one needs to determine an infinite number of correlation functions:

$$\langle h(\mathbf{x})h(\mathbf{x}')\rangle, \quad \langle h(\mathbf{x})h(\mathbf{x}')h(\mathbf{x}'')\rangle, \quad ...$$

For randomly rough surfaces all the statistical properties of the surface are already contained in the lowest-order correlation function:

$$C(\mathbf{x}, \mathbf{x}') = \langle h(\mathbf{x})h(\mathbf{x}')\rangle \tag{1}$$

In this case, all correlation functions with an odd number of height coordinates $h(\mathbf{x})$ vanish, and those with an even number of height coordinates can be written as products of the pair correlations function (1) (see Appendix A in Ref. [14]). Randomly rough surfaces have Gaussian height probability distributions which are not observed for all surfaces of engineering interest but are good approximations in many cases, such as for sandblasted surfaces or surfaces produced by crack propagation. In analytical contact mechanics theories using the top power spectrum one can often obtain useful results for the contact between surfaces with non-Gaussian roughness. The top power spectrum replaces the roughness below the average plane with the same type of roughness as above the average plane and is useful in contact mechanics applications where the contact only occurs between the bodies in the upper half of the roughness profile [14].

If the statistical properties of the surface are translational invariant, the correlation function (1) only depends on the coordinate difference $\mathbf{x} - \mathbf{x}'$, and no information will be lost if we put $\mathbf{x}' = \mathbf{0}$ in (1). For such systems, it is more useful to study the correlation function (1) in wavevector space $\mathbf{q} = (q_x, q_y)$ with the 2D surface roughness power spectrum defined as:

$$C_{2D}(\mathbf{q}) = \frac{1}{(2\pi)^2}\int d^2x\, \langle h(\mathbf{x})h(\mathbf{0})\rangle e^{i\mathbf{q}\cdot\mathbf{x}} \tag{2}$$

For surfaces with roughness with isotropic properties, $C_{2D}(\mathbf{q})$ depends only on the magnitude $q = |\mathbf{q}|$ of the wave vector.

In calculating power spectra $C_{2D}(\mathbf{q})$ from measured topography data, instead of using (2) it is more convenient to use the Fast Fourier Transform Method to first calculate the height in wavevector space:

$$h(\mathbf{q}) = \frac{1}{(2\pi)^2}\int_{A_0} d^2x\, h(\mathbf{x})e^{-i\mathbf{q}\cdot\mathbf{x}}$$

from which one can obtain [14]

$$C_{2D}(\mathbf{q}) = \frac{(2\pi)^2}{A_0}|h(\mathbf{q})|^2,$$

where $A_0 = L_0^2$ is the studied surface area.

Randomly rough surfaces can be obtained by adding plane waves with random phases:

$$h(\mathbf{x}) = \sum_{\mathbf{q}} B_q e^{i\mathbf{q}\cdot\mathbf{x}+i\phi_q}, \tag{3}$$

where ϕ_q are random numbers uniformly distributed between 0 and 2π. The parameter B_q in (3) can be written as $B_q = (2\pi/L)[C_{2D}(\mathbf{q})]^{1/2}$.

The power spectrum (2) is of course also defined for surfaces with non-random roughness and can be used to express many physical quantities. For example, when an elastic solid (with Young's modulus E and Poisson ratio ν) is squeezed into complete contact with a rough but nominally flat rigid surface, the elastic energy stored at the interface due to the deformations induced by the surface roughness is given by:

$$U_{el} = \frac{1}{2}E^*A_0\int d^2q\, qC_{2D}(\mathbf{q}), \tag{4}$$

where A_0 is the nominal surface area and $E^* = E/(1-\nu^2)$ is the effective Young's modulus, and we have assumed no interfacial friction. Other important quantities determined by $C_{2D}(\mathbf{q})$ are the root-mean-square (rms) roughness h_{rms} and the rms slope ξ:

$$h_{\rm rms}^2 = \langle h^2 \rangle = \int d^2q\, C_{\rm 2D}(\mathbf{q}) \tag{5}$$

$$\xi^2 = \langle (\nabla h)^2 \rangle = \int d^2q\, q^2 C_{\rm 2D}(\mathbf{q}) \tag{6}$$

The parameters $h_{\rm rms}$ and ξ are usually denoted $S_{\rm q}$ and $S_{\rm dq}$.

A randomly rough surface has a Gaussian height probability distribution:

$$P_h = \frac{1}{(2\pi)^{1/2} h_{\rm rms}} e^{-(h/h_{\rm rms})^2/2}. \tag{7}$$

This equation implies that for an infinite system, there will be arbitrary high surface points. However, for any finite system, the probability of finding very high surface points is small. Non-random surfaces usually have non-Gaussian height probabilities, and for such surfaces skewness and kurtosis are very useful quantities that are defined as:

$$S_{\rm sk} = \frac{\langle h^3 \rangle}{\langle h^2 \rangle^{2/3}}, \quad S_{\rm ku} = \frac{\langle h^4 \rangle}{\langle h^2 \rangle^2}, \tag{8}$$

where

$$\langle h^n \rangle = \int_{-\infty}^{\infty} dh\, h^n P_h$$

For randomly rough surfaces (P_h is Gaussian), $S_{\rm sk} = 0$ and $S_{\rm ku} = 3$.

3 Surface Roughness Power Spectra: Theory

The 2D power spectrum can be calculated from the height coordinate of a surface $z = h(\mathbf{x})$ with $\mathbf{x} = (x, y)$, which is assumed given in $N \times N$ data points (typically $N = 512$ or 1024). The studied surface area may be part of the surface of a curved body but we assume that the macroscopic curvature is removed so that $\langle h \rangle = 0$. As discussed above, the roughness profile $z = h(\mathbf{x})$ of a randomly rough surface can be written as a sum of plane waves $e^{i\mathbf{q}\cdot\mathbf{x}}$ with different wave vectors $\mathbf{q}$. The wavenumber $q = |\mathbf{q}| = 2\pi/\lambda$, where λ is the wavelength of one roughness component.

The most important property of a rough surface is its 2D power spectrum (2). Assuming that the surface has isotropic statistical properties, $C_{\rm 2D}(\mathbf{q})$ depends only on the magnitude $q = |\mathbf{q}|$ of the wave vector. A self-affine fractal surface has a power spectrum $C_{\rm 2D}(q) \sim q^{-2(1+H)}$, (where H is the Hurst exponent related to the fractal dimension $D_{\rm f} = 3 - H$), which is a straight line with the slope $-2(1 + H)$ when plotted on a log-log scale. Most solids have surface roughness with the Hurst exponent $0.7 < H < 1$ (see Ref. [34]).

For a one-dimensional (1D) line scan $z = h(x)$, one can calculate the 1D power spectrum defined by:

$$C_{\rm 1D}(q) = \frac{1}{2\pi} \int_{-\infty}^{\infty} dx\, \langle h(x)h(0) \rangle e^{iqx} \tag{9}$$

Since $\langle h(x)h(0) \rangle \to \langle h(x) \rangle \langle h(0) \rangle = 0$ as $|x| \to \infty$ this integral is usually well-defined and in most cases, the limits $\pm\infty$ can be replaced by $\pm L/2$, where L is the length of the line over which the topography was measured. We note that most engineering surfaces have power spectra with long wavelength roll-off regions (say for the wavenumber $q < q_{\rm r}$), and for such surfaces, it is enough to measure $h(x)$ over a length a few times $1/q_{\rm r}$.

Using (2) and (9) it is easy to show that the mean-square (ms) roughness

$$\langle h^2 \rangle = h_{\rm rms}^2 = 2\pi \int_0^{\infty} dk\, k C_{\rm 2D}(k) = 2 \int_0^{\infty} dk\, C_{\rm 1D}(k) \tag{10}$$

If we assume the surface has self-affine fractal roughness, the power spectrum can be written as

$$C_{\rm 2D}(q) = C_0 q^{-2-2H}$$

which is defined for $q_0 < q < q_1$, and zero otherwise, then using (10) we get

$$h_{\rm rms}^2 = 2\pi \int_{q_0}^{q_1} dk\, C_0 k^{-1-2H} \approx \frac{\pi}{H} C_0 q_0^{-2H},$$

where we have assumed $q_1/q_0 >> 1$ and $H > 0$, thus

$$C_{\rm 2D} = \frac{H}{\pi} h_{\rm rms}^2 \frac{1}{q_0^2} \left(\frac{q}{q_0} \right)^{-2-2H} \tag{11}$$

In a similar way using (9) and (10) we get

$$C_{\rm 1D} = H h_{\rm rms}^2 \frac{1}{q_0} \left(\frac{q}{q_0} \right)^{-1-2H} \tag{12}$$

Note that $C_{\rm 1D} = \pi q C_{\rm 2D}$ but this relation only holds exactly when $C_{\rm 2D}$ is a power law in the wavenumber q (see below).

For surfaces with isotropic roughness the 2D power spectrum $C_{\rm 2D}(q)$ can be obtained directly from $C_{\rm 1D}(q)$ (see [35]):

$$C_{\rm 2D}(q) = \frac{1}{\pi} \int_q^{\infty} dk\, \frac{[-C'_{\rm 1D}(k)]}{\left(k^2 - q^2\right)^{1/2}} \tag{13}$$

This relation for calculating the 2D power spectrum from the 1D power spectrum is very useful. The related relation on how to obtain the 1D power spectrum from the 2D power spectrum is less useful [11]:

$$C_{1D}(q) = 2\int_q^\infty dk\,\frac{kC_{2D}(k)}{\left(k^2-q^2\right)^{1/2}} \tag{14}$$

If $C_{1D}(q)$ is obtained from line scan measurements it is known only numerically. And since it is in general a noisy function of the wavenumber q, the derivative $C'_{1D}(q)$ will typically fluctuate wildly with q making the relation (13) not very useful in many practical applications unless $C_{1D}(q)$ can be fitted by a smooth function.

Equations (13) and (14) are exact and must hence obey the "sum rule" (10). To demonstrate that, taking (13) as an example, we calculate

$$\begin{aligned} I =& 2\pi\int_0^\infty dq\,qC_{2D}(q)\\ =& 2\pi\int_0^\infty dq\,q\frac{1}{\pi}\int_q^\infty dk\,\frac{[-C'_{1D}(k)]}{\left(k^2-q^2\right)^{1/2}} \end{aligned}$$

Writing $k = qx$ this gives

$$\begin{aligned} I =& 2\int_0^\infty dq\,q\int_1^\infty dx\,\frac{[-C'_{1D}(qx)]}{\left(x^2-1\right)^{1/2}}\\ =& 2\int_1^\infty dx\,\frac{1}{\left(x^2-1\right)^{1/2}}\int_0^\infty dq\,q[-C'_{1D}(qx)] \end{aligned}$$

Defining $qx = y$ this gives

$$I = 2\int_1^\infty dx\,\frac{1}{x^2\left(x^2-1\right)^{1/2}}\int_0^\infty dy\,y[-C'_{1D}(y)]$$

Using partial integration and assuming that $yC_{1D}(y)$ vanishes for $y = 0$ and $y = \infty$ we get

$$I = 2\int_0^\infty dy\,C_{1D}(y) = h_{rms}^2,$$

where we have used that

$$\int_1^\infty dx\,\frac{1}{x^2\left(x^2-1\right)^{1/2}} = 1$$

an equation that is easy to prove by changing the integration variable using $x = 1/\cos\phi$. Similarly, one can show that (14) satisfies the sum rule (10).

There are two other way to calculate $C_{2D}(q)$ approximately from $C_{1D}(q)$. For a self-affine fractal surface (without a roll-off) fitting $C_{1D}(q)$ with (12) gives the Hurst exponent H and the rms roughness h_{rms} and knowing these parameters from (11) we can calculate $C_{2D}(q)$ (see also Appendix A).

A second way is as follows. First note that the mean square (ms) roughness amplitude can be obtained from $C_{1D}(q)$ and $C_{2D}(q)$ via (10). If the topography is measured with an instrument with finite resolution then only wavenumbers below some value $q = 2\pi/\lambda$ can be resolved. In that case, one would observe an apparent ms roughness

$$h_{rms}^2 \approx 2\pi\int_0^q dk\,kC_{2D}(k) \approx 2\int_0^q dk\,C_{1D}(k)$$

In this equation, q can be considered as a parameter (depending on the instrument resolution) so we can take the derivative with respect to q to get

$$2\pi qC_{2D}(q) \approx 2C_{1D}(q)$$

or

$$C_{2D}(q) \approx \frac{1}{\pi q}C_{1D}(q) \tag{15}$$

which is the same result as found previously by comparing (11) and (12). However, this relation is in general only approximate and the exact relation is given by (13). Note in particular if $C_{1D}(q)$ has a roll-off region for $q < q_r$, where C_{1D} is approximately constant, then from (15) we get in the roll-off region $C_{2D} \sim 1/q$ while the exact result (13) for $q << q_r$ gives

$$C_{2D}(q) \approx \frac{1}{\pi}\int_{q_r}^{q_1} dk\,\frac{1}{k}[-C'_{1D}(k)]$$

which is constant. Thus if (15) is used for a self-affine fractal surface with a roll-off, one should replace the $\sim 1/q$ region with a constant determined by C_{2D} at the onset $q = q_r$ of the roll-off region (here q_r refers to the largest wavenumber q of the $\sim 1/q$ region). In addition the magnitude of $C_{2D}(q)$ given by (15) in the self-affine fractal region must be corrected (scaled) by a factor $\approx (1+3H)^{1/2}$ which depends on the Hurst exponent H (see Appendix A). This correction factor is needed in order for the sum rule (10) to be satisfied: decreasing $C_{2D}(q)$ in the roll-off region imply we must increase $C_{2D}(q)$ in the self-affine fractal region in order for the sum rule to be obeyed. Note that the onset of the roll-off region occurs at the same wavenumber q_r for $C_{1D}(q)$ and $C_{2D}(q)$ (see vertical dashed line in Fig. 2). In most practical applications, the detailed form of the power spectrum in the roll-off region is not very important (but the fact that a roll-off region exists for $q < q_r$ is very important).

To illustrate the discussion above we have calculated the power spectrum for a randomly rough surface obtained by adding plane waves with random phases (see (3) and Appendix A in Ref. [14]). Fig. 1 shows a mathematically generated randomly rough surface with the rms roughness $h_{rms} = 1$ μm and Hurst exponent $H = 0.8$. The small, large and roll-off wavenumbers are $q_0 = 1\times10^3$ m^{-1}, $q_1 = 2048\times10^3$ m^{-1} and $q_r = 30\times10^3$ m^{-1}, respectively. The surface consists of 2048×2048 height data points.

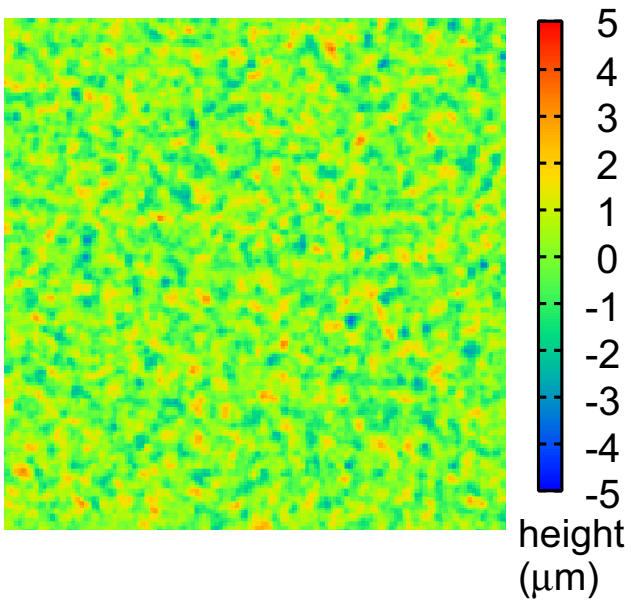

Fig. 1 A mathematically generated randomly rough surface with the rms roughness $h_{\rm rms} = 1$ µm and Hurst exponent $H = 0.8$. The small, large and roll-off wavenumbers are $q_0 = 1 \times 10^3$ m^{-1}, $q_1 = 2048 \times 10^3$ m^{-1} and $q_{\rm r} = 30 \times 10^3$ m^{-1}, respectively

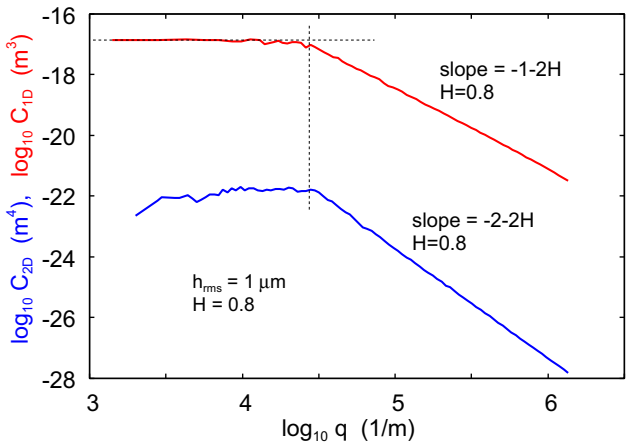

Fig. 2 The 1D (red line) and 2D (blue line) power spectra calculated from a mathematically generated randomly rough surface with the rms roughness $h_{\rm rms} = 1$ µm and Hurst exponent $H = 0.8$. The small, large and roll-off wavenumbers are $q_0 = 1 \times 10^3$ m^{-1}, $q_1 = 2048 \times 10^3$ m^{-1} and $q_{\rm r} = 30 \times 10^3$ m^{-1}, respectively

Fig. 2 shows the 1D (red line) and 2D (blue line) power spectra calculated from the height profile $z = h(x, y)$ of the surface shown in Fig. 1. The 1D power spectrum is the average of C_{1D} over all 2048 $z = h(x)$ (y constant) lines contained in the height profile $z = h(x, y)$.

The red line in Fig. 3 shows the input power spectrum used to generate the surface shown in Fig. 1. The blue line is the power spectra calculated from the rough surface using the 2D power spectrum equation (2). The green line is the

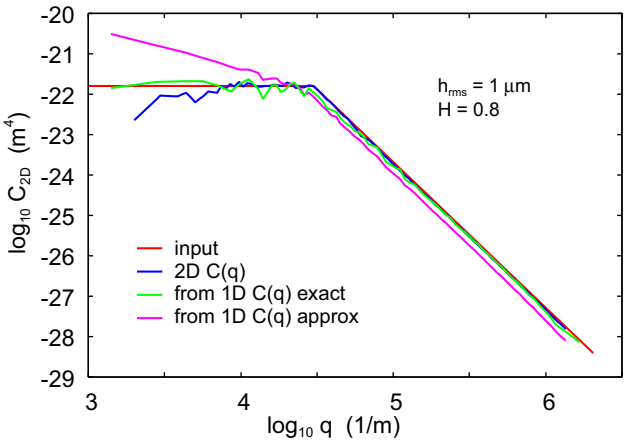

Fig. 3 The input power spectrum is used to generate the surface topography of a randomly rough surface (red line), and the power spectra calculated from the rough surface using the 2D power spectrum equation (blue line), using (13) with the 1D power spectrum calculated from the rough surface (red line in Fig. 2) (green line) and using the approximate equation (15) (pink line)

2D power spectrum obtained from the 1D power spectrum (given by the red line in Fig. 2) using the (exact) equation (13), while the pink line is calculated using the approximate equation (15). Note that the approximate formula (15) gives a linear dependency of $1/q$ in the roll-off region in contrast to the nearly constant value resulting from the exact equation (13). Additionally, in the self-affine fractal region, the power spectrum as described by (15) is underestimated by a factor of $\approx (1 + 3H)^{1/2}$. For $H = 0.8$, this factor is approximately 1.84 (see Appendix A).

4 Surface Roughness Power Spectra: Experiment

Using optical and stylus measurements, we have studied the surface topography on two types of samples supplied by the Surface Topography Challenge [36]. We refer to these two types as the "rough" and "smooth" surfaces. In this study, six smooth samples: B54, B55, C13, C14, A71, A72 and five rough samples: R54, P85, P86, P63, P64 were used. The same samples were prepared on one single wafer and subsequently cut into 1 cm × 1 cm pieces, so theoretically they should have similar surface characteristics.

Both smooth and rough samples have coatings made from chromium nitride (CrN). The smooth surface has CrN deposited on a prime-grade polished silicon wafer, while the rough surface has CrN deposited on the rough "backside" of a single-side-polished silicon wafer, which has been subsequently etched with isotropic reactive ions. CrN was chosen because it is a wear-and-corrosion-resistant coating which is widely used in automotive components, cutting tools, and

die-casting. CrN is typically deposited via physical vapor deposition (PVD), and the present deposition uses a magnetron sputtering technique. The silicon substrates were chosen due to their extreme reproducibility in fabrication. The two substrates are intended to produce a "smooth surface" that is representative of materials used in the semiconductor industry, and a "rough surface" that has larger topographic variation, as is common in other industrial contexts.

4.1 Engineering Stylus

The topography measurements were performed using two stylus profilometers:

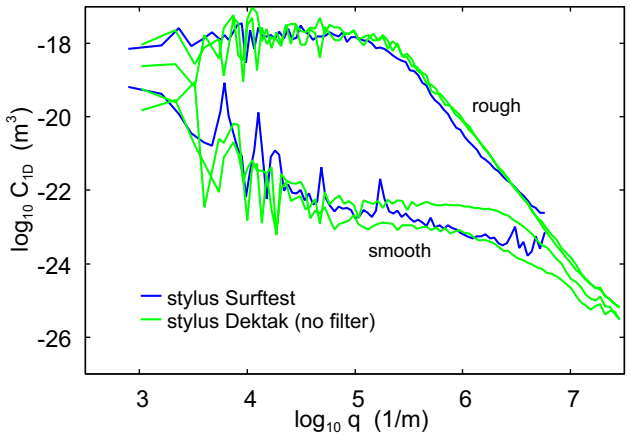

Fig. 4 The 1D surface roughness power spectra of the smooth and rough surfaces calculated from topography data obtained using two different engineering stylus instruments. The blue lines are the Surftest stylus data while the green lines are using another (Dektak) stylus instrument. The two green lines for the smooth and rough surfaces were obtained on different sample surfaces (samples B55 and C13 for the smooth surface and R54 and P86 for the rough surface)

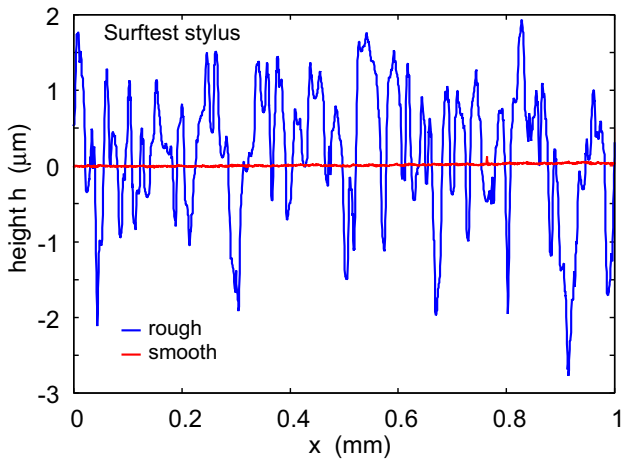

Fig. 5 The height $h(x)$ as a function of x for the smooth (red) and rough (blue) surfaces as obtained using the Surftest stylus instrument

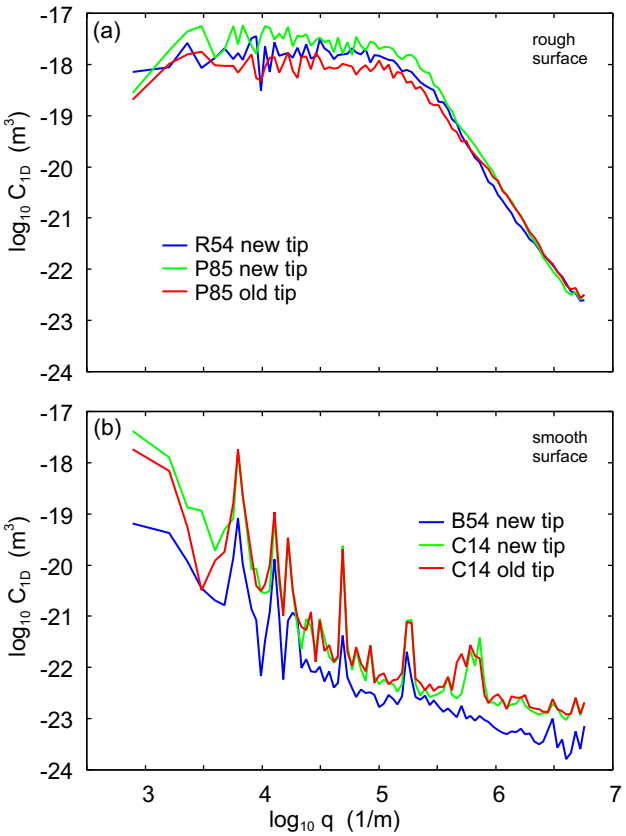

Fig. 6 The power spectrum calculated from the Mitutoyo topography data for the samples R54 (rough) and B54 (smooth) (blue lines, from Fig. 4) and for the surfaces P85 (rough) and C14 (smooth) using an old (red lines) and new (green lines) diamond tip. The old tip was used for several years (for several 100 topography measurements) before performing the measurements reported here

(a) A Mitutoyo Portable Surface Roughness Measurement Surftest SJ-410 equipped with a diamond tip having a radius of curvature $R = 1$ μm, and with the tip-substrate repulsive force $F_N = 0.75$ mN. The step length (pixel) is 0.5 μm, the scan length $L = 8$ mm and the tip speed $v = 50$ μm/s. The

power spectra shown in Fig. 4 (blue lines) were obtained by averaging over three measurements on each surface.

(b) A Bruker Dektak XT, equipped with a diamond tip having a radius of curvature $R = 0.7$ μm, and with the tip-substrate repulsive forces $F_N = 1 \times 10^{-5}$ N and 2×10^{-5} N. The scan lengths were $L = 3$ and 6 mm with steps resolutions of 0.15 and 0.10 μm, respectively. The tip speed varied between 33 and 44 μm/s. The Bruker Dektak was mounted on a vibration isolation table.

The blue and green lines in Fig. 4 are the 1D surface roughness power spectra of the smooth and rough surfaces obtained with the Mitutoyo and Bruker stylus instruments, respectively. The two green lines for the smooth and rough surfaces were obtained on different sample surfaces (samples B55 and C13 for the smooth surface and R54 and P86 for the rough surface). In our original measurement with the Brucker stylus, a short wavelength filter was included which resulted in large deviations between the two stylus measurements for large wavevectors (not shown). In the Mitutoyo case, no filter was used. Filters are used to make some quantities, such as the rms slope, more well-defined[1]. However, many physical quantities, such as the area of real contact, depend on the short wavelength roughness. Therefore, *no filter should be used in calculating power spectra that are intended for theoretical calculations*.

Figure 5 shows the height $h(x)$ as a function of x for the smooth (red) and rough (blue) surfaces as obtained using the Surftest stylus instrument.

Figure 6 shows the power spectrum calculated from the Mitutoyo data for the samples R54 (rough) and B54 (smooth) (blue lines, from Fig. 4) and for the surfaces P85 (rough) and C14 (smooth) using an old (red lines) and new (green lines) diamond tip. The old tip was used for several years (for several hundred topography measurements) before performing the measurements reported here. The blue curve in Fig. 6 was measured on B54 (smooth wafer) ~ 1/2 year after the measurements of the red and green curves. For the C14 surface the old and the new tips give nearly the same power spectra which indicates that wear (or contaminations) on the tips has a negligible influence on the measured topography.

4.2 Atomic Force Microscopy (AFM)

We have used two AFM setups in the present study:

(a) A Bruker Dimension 3100 AFM in tapping mode (amplitude modulation) equipped with RSTESPA-300 probe having a 8 nm tip radius. Two 2D scan pixel numbers were used: 512×512 and 1024×1024. The scanned areas were as follows: 5×5 μm^2 for the smooth surfaces, and 40×40 μm^2 for the rough surfaces. The reason for a larger scan length of the rough surfaces was to have a good average over the observed "plateau" topography features. Figure 7 shows AFM topography images obtained with setup (a) for rough and smooth samples.

(b) Veeco Multimode IIIA AFM in tapping mode. Three silicon ContAl-G cantilever probes (BudgetSensors,

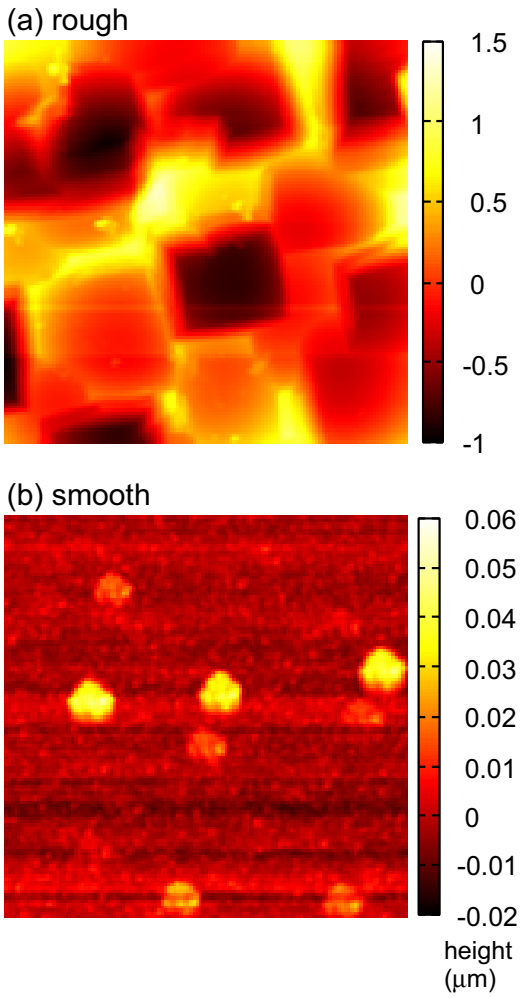

Fig. 7 AFM pictures of the rough and the smooth surfaces. The studied unit is 40×40 μm^2 for the rough surface and 5×5 μm^2 for the smooth surface. The square units in **a** have the linear size ~ 10 μm

[1] On a Bruker Dektak XT info page, one can read: "The power of proper filtering for data analysis, according to recognized ISO standard methods, cannot be overestimated when striving to provide the most accurate and reproducible results for a measuring system" and "The short cutoff filter with a cutoff spatial frequency of λ_s is applied to this total profile in order to produce the "primary profile". The spatial frequencies that are rejected by the short cutoff are considered noise ... " Filters are used for several purposes: (a) to make some quantities, like the rms slope, more well-defined or (b) to eliminate undesired vibrations of the tip during the scan. (See, ISO-Standardized Filtering for DektakXT Stylus Profilers, Application Note 550, Matt Novak and Son Bui, Bruker Nano Surfaces Division, Tucson, AZ USA.) However, it is often possible to avoid tip vibration by tuning the contact force and scan speed. In general, filtering should never be used if the topography is used as input for theory calculations

Bulgaria) were used in the measurements, one for sample A71, one for A72 and P63, and one for P64. The cantilevers have resonance frequencies of ~ 14 kHz, the spring constants of ~ 0.2 N/m, and tip apex radii of ~ 10 nm. The scanning setpoints and the feedback parameters were manually optimized for each imaging. For the smoother A71 and A72 samples, multiple topographies were measured with scan sizes of 0.512, 1.024, 2.048, 5.12, 10.24, 25.6 μm. For the rougher P63 and P64 samples, two additional larger scan sizes of 51.2 and 102.4 μm were also included. The scan rates used in the measurements are 3 lines/s for scan sizes of 0.512 μm, 2 lines/s for scan sizes of 1.024, 2.048 μm, and 1 line/s for others. All the measured topography images have data points of 512 × 512 pixels. Figure 8 shows AFM topography images obtained with setup (b) for rough and smooth samples at different scan sizes.

Figure 9 shows the 1D power spectra calculated from the AFM topography data obtained with setup (a), for two measurements on the rough surface and one measurement on the smooth surface. In all cases, the topography was measured in 1024 × 1024 points. Note that the AFM data overlap the stylus measurements in the region of common wavenumber. This is a good test which shows that both measurement methods are accurate. Note also that the power spectra of the two surfaces for wavenumber $q > 3 \times 10^7$ m^{-1} (or wavelength below $\lambda = 2\pi/q \approx 200$ nm) appear to be nearly the same which may reflect some intrinsic roughness of the CrN coating independent of the substrate roughness. This is confirmed by AFM at higher resolution (Fig. 8), which shows nearly the same topography for the smooth and rough surfaces at the highest resolution. Note that the short wavelength roughness of the substrate (with a wavelength much smaller than the thickness of the coating) may not show up at the surface of the coating film.

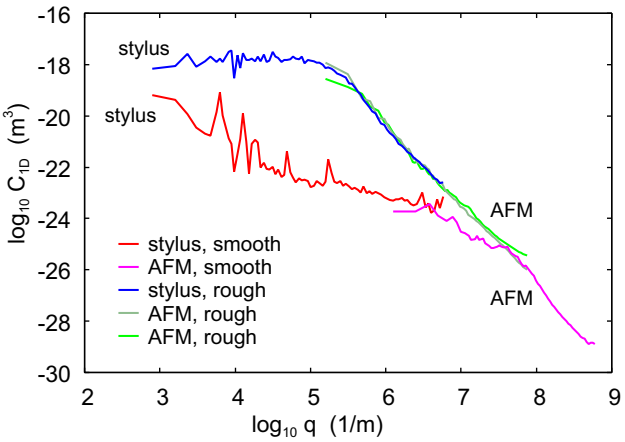

Fig. 9 The 1D surface roughness power spectra of the smooth and rough surfaces calculated from topography data obtained using an engineering stylus instrument (red and blue curves), and AFM setup (**a**). The stylus power spectrum was obtained by averaging the power spectra obtained from 3 line scans each 8 mm long. The AFM data consisted of 1024 × 1024 data points. For the AFM data, the 1D power spectrum was calculated for each $z = h(x)$ line and averaged over all the 1024 lines

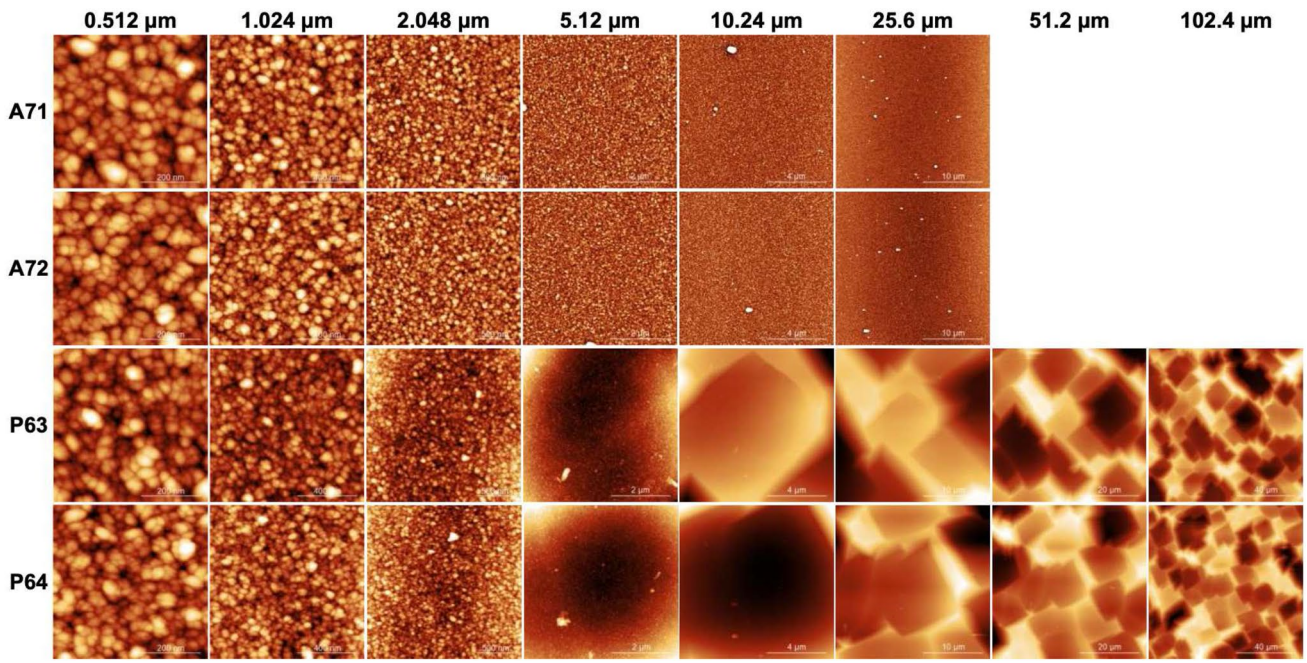

Fig. 8 AFM topography images at different scan sizes for smooth (A71, A72) and rough (P63, P64) surfaces

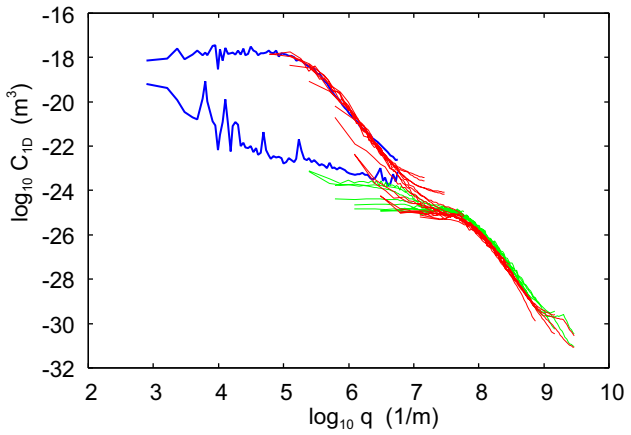

Fig. 10 The 1D surface roughness power spectra of the smooth and rough surfaces calculated from topography data obtained using an engineering stylus instrument (blue curves), and AFM setup (**b**). The stylus power spectrum was obtained by averaging the power spectra obtained from 3 line scans each 8 mm long. The AFM data consisted of 512 × 512 data points. For the AFM data, the 1D power spectrum was calculated for each $z = h(x)$ line and averaged over all the 512 lines

Figure 10 shows the 1D surface roughness power spectra of the smooth and rough surfaces calculated from topography data obtained using an engineering stylus instrument (blue curves from Fig. 4), and the AFM setup (b). The stylus power spectrum was obtained by averaging the power spectra obtained from 3 line scans each 8 mm long. For the AFM data the 1D power spectrum was calculated for each $z = h(x)$ line and averaged over all the 512 lines.

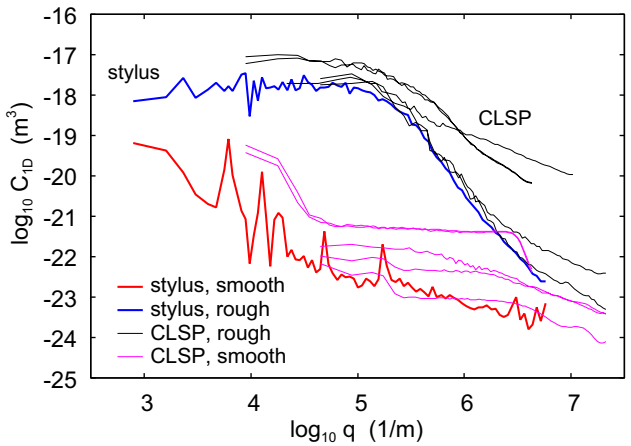

Fig. 11 The 1D surface roughness power spectra of the smooth and rough surfaces calculated from topography data obtained using an engineering stylus (red and blue curves), and 3D Confocal Laser Scanning Profilometry (CLSP). The CLSP was performed in 1024 × 768 data points

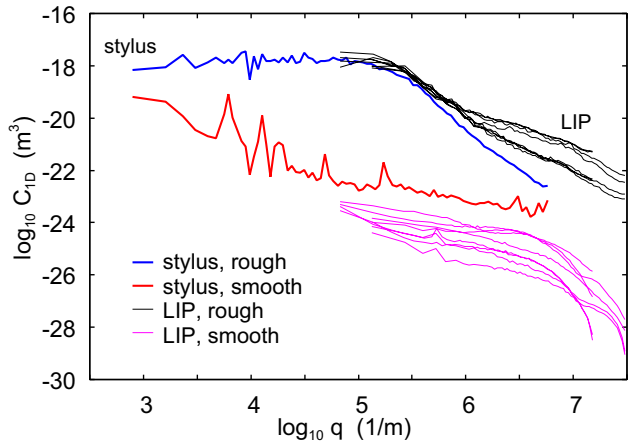

Fig. 12 The 1D surface roughness power spectra of the smooth and rough surfaces calculated from topography data obtained using an engineering stylus (red and blue curves), and Light Interferometry Profilometry (LIP). The LIP was performed in 480 × 640 data points

4.3 Confocal Laser Scanning Profilometry (CLSP)

The laser profilometry was performed using two different instruments: Keyence VK-X1050 and Keyence VK-3000. Both instruments have magnifications of 10, 20, 50, and 100×. A red 661 nm laser beam was used and the pixel number was 768 × 1024. Figure 11 compares the $C_{1D}(q)$ results from the CLSP to the output from engineering stylus for the rough and smooth surfaces.

4.4 Light Interferometry Profilometry (LIP)

A white and green 3D light interferometry profilometer Veeco NT-9100, with a 50× magnification was used to study the surface topography of smooth and rough samples.

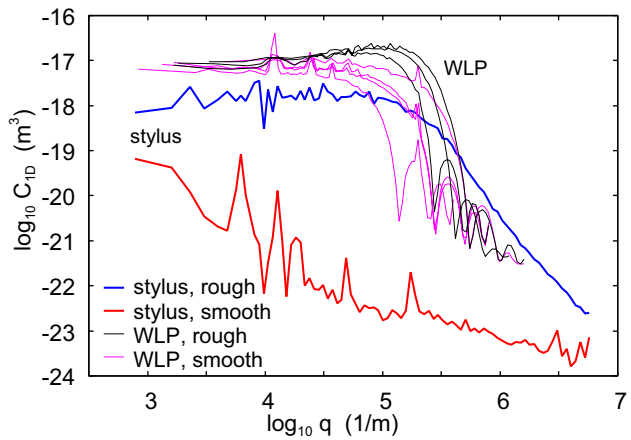

Fig. 13 The 1D surface roughness power spectra of the smooth and rough surfaces calculated from topography data obtained using an engineering stylus (red and blue curves), and White Light Profilometry (WLP). The WLP was performed in 1418 × 1392 data points

The scanned area was 94×50 μm^2 with the pixel number 640×480. Figure 12 compares the $C_{1D}(q)$ results from the LIP to the output from engineering stylus for the rough and smooth wafers.

The optically obtained power spectra in Figs. 10 and 11 extend to $q \approx 3 \times 10^7$ m^{-1} corresponding to the wavelength ~ 0.1 μm. This is shorter than the wavelength of the used light and it is clear that the large wavenumber region ($q > 3 \times 10^6$ m^{-1}) cannot be trusted. However, our study shows that even for much smaller wavenumbers the optical methods fail to correctly describe the power spectra.

4.5 White Light Profilomtry (WLP)

We have used a 3D Optical Profilometer (Keyence VR6200) to perform non-contact measurement with a stated resolution of 0.1 μm. Measurements were performed as follows: (a) Single scan magnifications of 40, 80, and 120× and scan pixel number of 768×1024. (b) Stitch mode at 80× magnification at the scan pixel number 1392×1418 (rough surface) and 1108×1283 (smooth surface). Figure 13 compare the $C_{1D}(q)$ results from the WLP compared to the output from engineering stylus for the rough and smooth wafers.

5 Another Optical Method for Obtaining $C(q)$

We have shown that standard optical methods in general do not result in accurate surface roughness power spectra. They may approximately describe the long wavelength roughness, and may therefore result in good-looking topography pictures, but fail for the short wavelength roughness. However, for very smooth surfaces with roughness amplitude such that $k_0 h_{\rm rms} < 0.1$, where $k_0 = 2\pi/\lambda_0$ is the wavenumber of the light used, an essential exact way exist for obtaining $C(\mathbf{q})$ from light reflection data.

Based on the original work of Rayleigh [37], using first-order vector perturbation theory, Rice [38] and others have shown that for smooth enough surfaces the angular distribution of light scattered from a rough surface depends on the surface roughness only via the power spectrum $C(\mathbf{q})$, where $\mathbf{q}$ is the change in the photon wavevector in the xy-plane between the incident and reflected (scattered) photon beam:

$$\mathbf{q} = \mathbf{k}_\parallel - \mathbf{k}_\parallel^{(\rm i)} = (k_x - k_x^{(\rm i)}, k_y - k_y^{(\rm i)}),$$

where $\mathbf{k}$ is the wavevector of the scattered beam. The intensity of the light scattered into the solid-angle $d\Omega = \sin\theta d\theta d\phi$ is given by [39, 40]

Fig. 14 Laser light is reflected from a rough surface. The random granular pattern (speckles) is due to light reflection from the microscopic surface roughness and will look different when the laser beam is moved to another nominally identical surface region on the macroscopic body under study. The speckles disappear when the incident photon beam is incoherent

$$\frac{1}{I_{\rm i}}\frac{dI}{d\Omega} d\Omega \approx 4k_0^4 \cos\theta_{\rm i} \cos^2\theta \; Q \; C_{2D}(\mathbf{q}) d\Omega, \tag{16}$$

where $I_{\rm i}$ and $\theta_{\rm i}$ are the intensity of the incident beam and the angle of incidence, respectively, and where the factor Q depends on the incident and scattering angles and on the dielectric constant of the solid. Note the Rayleigh blue-sky factor k_0^4.

Assuming small scattering angles, (16) simplifies to

$$\frac{1}{I_{\rm s}}\frac{dI}{d\Omega} d\Omega \approx 4k_0^4 \cos^3\theta_{\rm i} \; C_{2D}(\mathbf{q}) d\Omega, \tag{17}$$

where $I_{\rm s} = RI_{\rm i}$ is the intensity of the reflected beam (R is the reflection factor and $I_{\rm i}$ the intensity of the incoming beam).

We have stated above that the $\langle .. \rangle$ in the definition of $C(\mathbf{q})$ stands for ensemble averaging. If no ensemble averaging is performed the $C(\mathbf{q})$ obtained from a single surface area will have some fine-scale noise reflecting the particular surface roughness occurring on the studied surface area. That is, without ensemble averaging $C(\mathbf{q})$ will have fine-scale speckle structure (noise) reflecting the surface area used. This speckle noise is well-known to anybody who has observed laser light reflected from surfaces where the term speckle refers to a random granular pattern that can be observed when a highly coherent light beam is diffusely reflected at a surface (see Fig. 14). This

phenomenon results from the interference of many different reflected portions of the incident beam with random relative optical phases. We note that if the incident beam is incoherent, speckle effects are automatically averaged out.

One interesting limiting case of (16) is for a one-dimensional (grating-like) roughness profile, $z = h(x)$, where

$$h(\mathbf{q}) = \frac{1}{(2\pi)^2}\int d^2x\, h(\mathbf{x})e^{-i\mathbf{q}\cdot\mathbf{x}} = \frac{1}{2\pi}\int dx\, h(x)e^{-iq_x x}\delta(q_y) = h(q_x)\delta(q_y)$$

Using that

$$|\delta(q_y)|^2 = \delta(q_y)\frac{1}{2\pi}\int dy\, e^{-iq_y y} = \frac{L_0}{2\pi}\delta(q_y),$$

where $A_0 = L_0^2$ is the studied surface area, we get

$$C_{2D}(\mathbf{q}) = \frac{(2\pi)^2}{A_0}|h(\mathbf{q})|^2 = \frac{2\pi}{L_0}|h(q_x)|^2\delta(q_y) = C_{1D}(q_x)\delta(q_y)$$

We substitute this in (16) and integrate over ϕ. To evaluate the ϕ-integral we use that $\sin\phi_i = 0$ (we assume the wavevector of the incident beam is in the xz-plane) and $q_y = k_0\sin\theta\sin\phi$ so that

$$\int_0^{2\pi} d\phi\, f(\phi)\delta(q_y) = \int_0^{2\pi} d\phi\, f(\phi)\delta(k_0\sin\theta\sin\phi) = \sum_{\phi=0,\pi}\frac{f(\phi)}{|k_0\sin\theta\cos\phi|} = \frac{f(0)+f(\pi)}{k_0\sin\theta} \tag{18}$$

Here we have used that $\sin\phi = 0$ for $\phi = 0$ and $\phi = \pi$. Using this result in (16) gives

$$\frac{1}{I_i}\frac{dI}{d\theta}d\theta \approx 8k_0^3\cos\theta_i\cos^2\theta\, Q\, C_{1D}(q_x)d\theta, \tag{19}$$

where $q_x = k_0\sin\theta\cos\phi = \pm k_0\sin\theta$ since $\phi = 0$ or $\phi = \pi$. However, $C_{1D}(q_x) = C_{1D}(-q_x)$ so we may use $q_x = k_0\sin\theta$. In (19) Q is evaluated for $\phi = 0$. Note that the $\sin\theta$ factor in $d\Omega$ cancels against the same factor occurring in the denominator in (17).

If $h(x) = h_0\sin(q_0x)$ we get

$$C_{1D}(q_x) = \frac{\pi}{2}\frac{h_0^2}{L_0}|\delta(q_x-q_0)-\delta(q_x+q_0)|^2 = \frac{h_0^2}{4}\left[\delta(q_x-q_0)+\delta(q_x+q_0)\right] = \frac{h_0^2}{4k_0}\left[\delta(q_x/k_0-q_0/k_0)+\delta(q_x/k_0+q_0/k_0)\right] \tag{20}$$

Using (19) and (20) gives the angular dependency of the scattered light from a sinus-grating.

Since the incident photon beam has the wavevector in the xz-plane we have $k_x^{(i)} = k_0\sin\theta_i$ and since $k_x^{(s)} = k_0\sin\theta_s$ we get

$$q_x/k_0 \pm q_0/k_0 = \sin\theta_s - \sin\theta_i \pm q_0/k_0$$

Thus, light incident on this surface profile will scatter in the form of a pair of first-order diffraction lines with positions determined by the familiar grating equation

$$\sin\theta_s = \sin\theta_i \pm q_0/k_0,$$

where $q_0/k_0 = \lambda_0/d$, where $d = 2\pi/q_0$ is the periodicity of the grating. The intensity of each of the grating lines are $\sim (k_0h_0)^2$ relative to the incident intensity. This limiting case illustrates that the intensity of the scattered light is determined by the square of the vertical amplitude of the roughness, while its angular spread is determined by the spatial wavelength of the roughness. The latter is easy to understand as the momentum is transferred to a photon by the grating is $\hbar\mathbf{q}$ to be compared to the incoming photon momentum $\hbar\mathbf{k}_0$.

The method described above has been applied successfully to obtain information about surface roughness using the scattering of laser light [40] and X-rays [41] from very smooth surfaces. However, we will now show that even the smooth surface studied above appears to be too rough for this method to be accurate.

5.1 X-Rays Reflectivity (XRR)

One of the smooth samples, C13, was analyzed using a Panalytical Empyrean Multipurpose X-ray diffractometer. The measurement was taken using Cu ka of wavelength 1.546 Å. The incident beam was shaped using a Bragg-Brentano

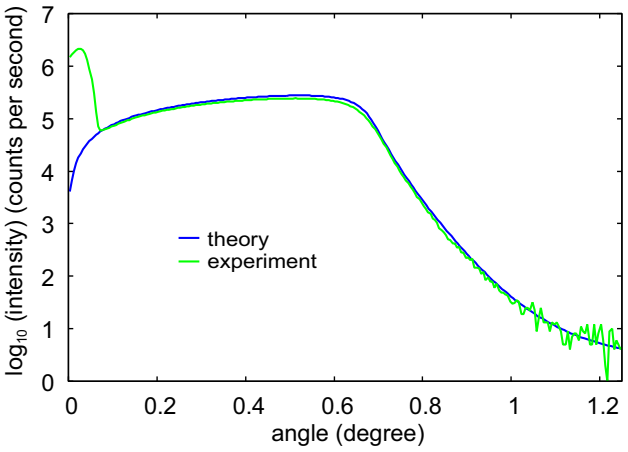

Fig. 15 The measured data (green) and the fitted (blue) specular reflectivity. The results for the height fluctuations and the assumed film thickness are given in the text

mirror and the reflected beam was detected using a Pixel-3D area detector in receiving mode with 1 of 255 channels active. Symmetric gonio scans were taken from 0 to 4° of 2θ with a step size of 0.005° 2θ and measurement speed of 0.44 s/step. The data were fitted in X'Pert Reflectivity (V1.3) software to estimate the mass density and the rms-roughness. Figure 15 shows the measured data (green) and the fitted model (blue). Assuming a 1.5 μm thick CrN film, the density obtained from the fitting was 5.85 gm/cm^3 and the roughness was 4.4 nm. Since the X-ray beam width was 6 mm, covering almost the full wafer dimension along the beam direction, the rms-roughness should be compared with the one obtained from the engineering stylus which is ~ 20 nm. AFM and XRR roughness measurements found in the literature show good agreement for surfaces with atomic-scale roughness and up to a few nanometers [41]. In our case, the smooth wafers appear too rough for the XRR method to be accurate.

6 Surface Roughness Parameters

The most complete information about surface roughness is the height probability distribution P_h and the surface roughness power spectrum $C(\mathbf{q})$. In Sec. 4 we showed the power spectra, and in Figs. 16, 17 and 18 we show the height probability distributions. Note that for the rough surface, all the stylus measurements give very similar P_h as expected when a large roll-off region is included in the measurements [12, 42]. This is not the case for the AFM data because it does not include a roll-off region. For the smooth surface, the Dektak stylus instrument gives very strongly fluctuating P_h while the Surftest gives a smoother curve which may, in part, result from the fact that the Dektak values are averages over only 3 lines.

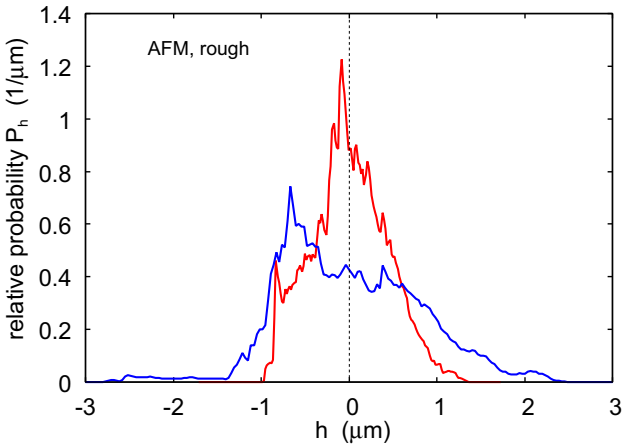

Fig. 17 The height probability distribution for the rough surface obtained using AFM

In most engineering applications just one or two parameters (numbers) are used, typically the rms roughness h_{rms} (or the arithmetic average) or maximum height of roughness Rz, are given to characterize the surface roughness. A very large number of surface roughness parameters have been defined [43] but in our opinion, only a few are really useful, namely h_{rms} and rms slope ξ, which can be obtained as integrals involving $C(\mathbf{q})$, and the the skewness S_{sk} and the kurtosis S_{ku}, which can be obtained as integrals involving P_h (see Sec. 2). The latter two parameters are important because they indicate to what extent a surface is randomly rough since in that case $S_{\mathrm{sk}} = 0$ and $S_{\mathrm{ku}} = 3$. (Note: if there is no roll-off region it is important to perform an average over many independent measurements (ensemble average) as otherwise the P_h, and hence also S_{sk} and S_{ku}, will fluctuate widely between different measurements.) The rms roughness h_{rms} is important for

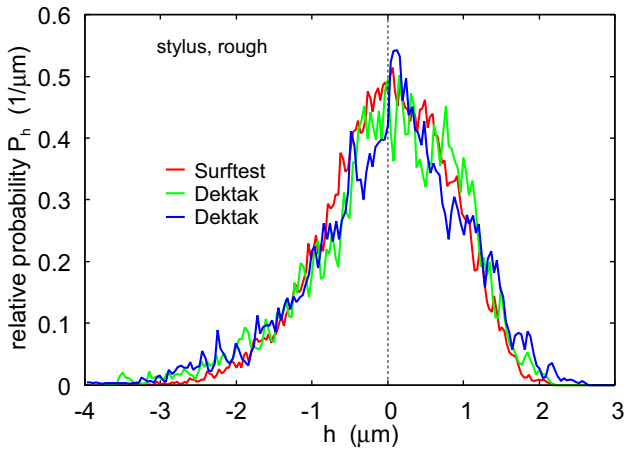

Fig. 16 The height probability distribution for the rough surface obtained using the engineering stylus instruments

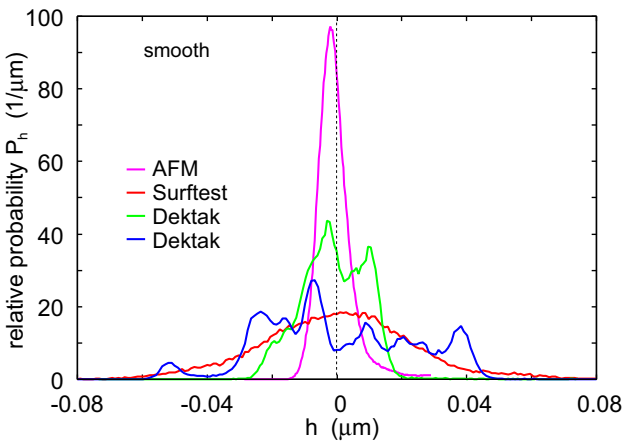

Fig. 18 The height probability distribution for the smooth surface obtained using AFM and the engineering stylus instruments

the average surface separation when two elastic solids are squeezed into contact while the rms slope ξ is important in a large number of applications, e.g., for determining the area of real contact between two elastic solids. In most cases $h_{\rm rms}$ depends mainly on the long wavelength roughness and is hence easy to measure using, e.g., an engineering stylus instrument if measured over a line long enough to cover the roll-off region of the power spectrum. The rms slope ξ depends on the short wavelength roughness, and to determine it, one may need to combine AFM with engineering line scan measurements to cover all relevant length scales.

7 On the Use of Calibration and Filters

Calibration is the comparison between measurement values delivered by a device under test with those of a calibration standard of known accuracy. For calibration of topography instruments, many calibration standards exist but most of them just specify the rms roughness (or rather the arithmetic average) and sometimes the lateral spacing distance in a periodic profile e.g., a sinus-like profile. To illustrate the problem with this, we show in Fig. 19 the power spectrum of a grit-blasted nickel surface which is used as a calibration standard. The supplier of this calibration standard states that it has the arithmetic average roughness Ra = 32 µinch or about 0.81 µm. Assuming that the rms-roughness is a factor of $(\pi/2)^{1/2}$ larger than Ra as expected for random roughness, this gives $h_{\rm rms} \approx 1$ µm. However, from the 20 mm long stylus topography measurement, we obtained $h_{\rm rms} \approx 10$ µm. This difference from what is expected must be due to the absence of filtering in our study. Figure 19 shows that the roughness on the calibration probe consists of short wavelength roughness separated by a roll-off region from the long wavelength roughness (usually denoted

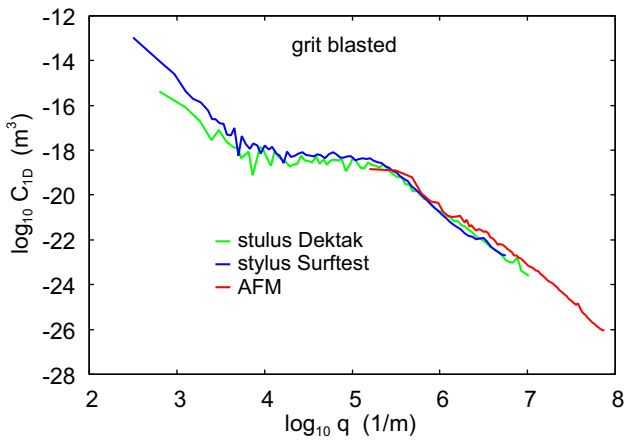

Fig. 19 The power spectrum of a grit blasted nickel surface (arithmetic average Ra = 32 µinch) supplied by Gar Electroforming [44] as a calibration standard

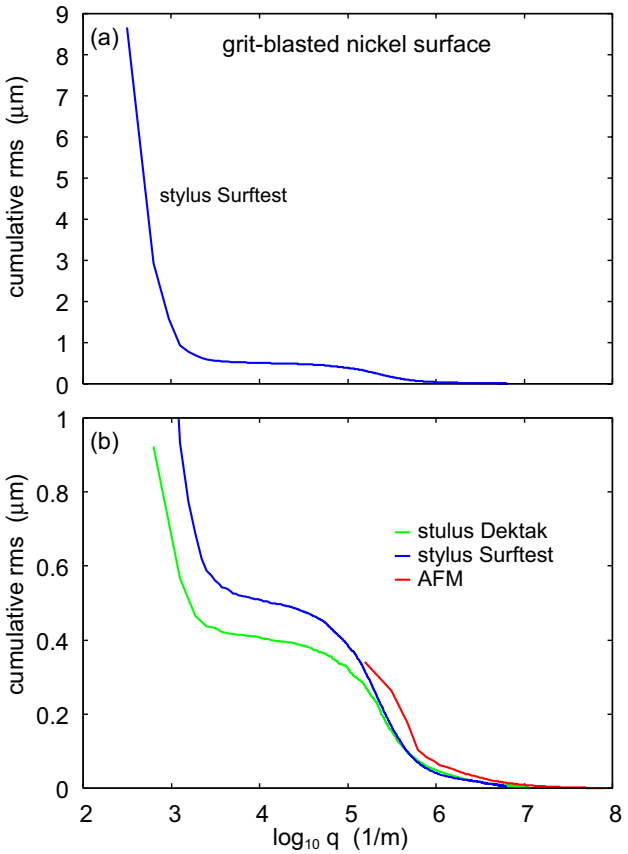

Fig. 20 The cumulative rms-roughness $h_{\rm rms}$ as a function of the small cut-off wavenumber. In the calculation of $h_{\rm rms}(q)$ only the roughness components with wavenumber between q and the large cut-off wavenumber q_1 (which equals 8×10^6 m^{-1} for the stylus measurement) is included in the calculation. **a** results using the Surftest stylus, and **b** the same as in **a** but including results from the Dektak stylus and the AFM. Results are obtained using (21) with the power spectra shown in Fig. 19

waviness), which extends to the linear size of the sample. Since the rms roughness $h_{\rm rms}$ usually is determined by the most long wavelength roughness components, removing the waviness may result in a much smaller rms-roughness in better agreement with the quoted roughness value.

To prove this assumption, in Fig. 20 we show the cumulative rms roughness $h_{\rm rms}(q)$ as a function of the small cut-off wavenumber q:

$$h_{\rm rms}^2(q) = 2\pi \int_q^{q_1} dq\, qC_{\rm 2D}(q) = 2 \int_q^{q_1} dq\, C_{\rm 1D}(q) \qquad (21)$$

Here q_1 is the largest wavenumber for which $C(q)$ is calculated. Figure 20a is obtained from the Surftest stylus, and shows that as q decreases towards q_0 (the smallest wavenumber for which $C(q)$ was measured) $h_{\rm rms}(q)$ increases to ≈ 9 µm. The most useful definition of the roughness amplitude excluding the waviness roughness region would

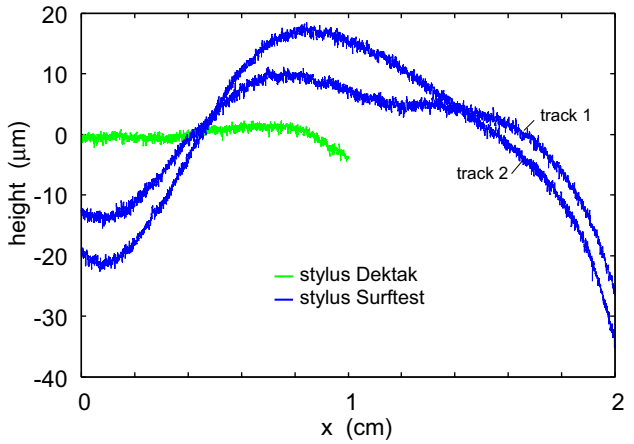

Fig. 21 Line scan tracks were obtained using the Surftest stylus (blue) and the Dektak stylus (green) after removing the average slope of the measured data but not the macroscopic curvature as the grit-blasted surface was nominally flat. The line scan data were used to calculate the power spectra in Fig. 19

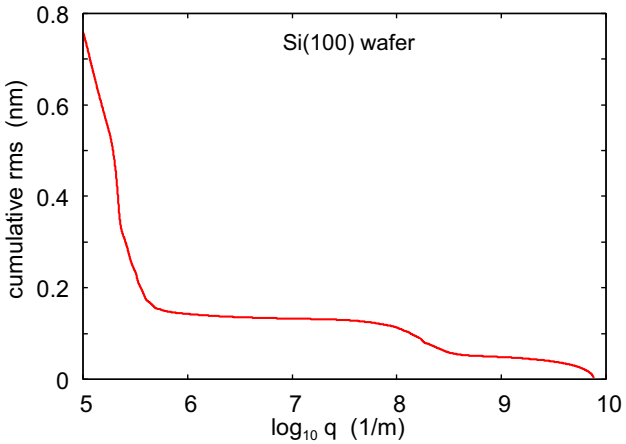

Fig. 22 The cumulative rms-roughness h_{rms} as a function of the small wavenumber cut-off based on AFM measurements from a Si(100) wafer [45]. In the calculation of $h_{rms}(q)$ only the roughness components with wavenumber between q and the large wavenumber cut-off q_1 (which equals 8×10^9 m^{-1}) is included in the calculation

be the value of $h_{rms}(q)$ in the roll-off region which is about ~ 0.5 μm [see Fig. 20b] which is somewhat smaller than the quoted roughness. This indicates that the quoted roughness must have been obtained with a filter removing most of the waviness.

Figure 20b shows the cumulative rms roughness obtained from the power spectra of the AFM and Dektak stylus instruments. Note that the Dektak stylus gives a smaller rms-roughness for small wavenumber q than the Surftest stylus. We attribute this to the shorter line scan length in the Dektak measurement. Thus, in calculating the power spectra and cumulative roughness we have only removed the slope (tilt) of the measured data, but not the macroscopic curvature as the grit blasted surface was nominally flat. This results in a larger long-range variation in the height for the Surftest stylus data when compared to the Dektak stylus data. This is supported by Fig. 21, where the line scan tracks obtained using the Surftest stylus (blue) and the Dektak stylus (green), used to calculate the power spectra in Fig. 19, are shown.

Removing the waviness using a filter is a very arbitrary and not useful approach as in some applications the long-wavelength roughness may be very important. This is often the case for the leakage of metallic seals, adhesion, or electric and thermal contact resistance. If information about the surface rms-roughness amplitude is important one should instead first calculate the power spectrum $C(q)$ (without filtering!!), from which one can obtain the rms-roughness [using (21)] including all relevant length scales. Similar length-scale dependent quantities, such as the rms slope, can also be obtained from integrals over $C(q)$ similar to (21).

Figure 19 shows good agreement between the AFM and the two stylus measurements, where the small difference (for a small wavenumber) between the two stylus results can be attributed to the different scan lengths. We have observed a similar agreement between the AFM and the stylus measurements for three other calibration standards where the surfaces were produced by lapping, grinding, and turning. In these cases, the stated Ra roughness is 0.05, 0.05, and 0.4 μm, respectively. But the roughness amplitudes we obtained including the waviness were much higher. A waviness region will occur on all smooth surfaces because it is nearly impossible to produce surfaces that are perfectly flat at the macroscopic length scale. This is the case even for wafers used in wafer bonding. Thus in Fig. 22 we show the cumulative rms roughness with decreasing small cut-off wavenumber for a Si(100) wafer obtained from AFM measurements. In Ref. [45] it was shown that the wafer waviness had negligible influence on wafer bonding, but in other applications, waviness can be very important.

8 Stylus Measurements on Soft Materials

For stylus measurements on soft solids, e.g., soft rubber materials, the tip-substrate force can effectively modify the real surface topography, as observed in Ref. [24] for silicone rubber (PDMS) where stick-slip occurred. However, replicas made with elastically stiff (glassy) polymer on soft (or hard) originals can be used to study the topography via stylus instruments.

Figure 23 shows schematically how a stylus tip may deform the surface of an elastically soft material. This could result in a measured topography that differs from the real one. However, if the deformations are the same everywhere as the tip is scanned over the surface, the measured topography will be the same as if the substrate is rigid. To prove it,

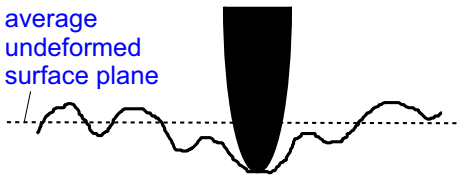

Fig. 23 The stylus tip deforms the material elastically but if the deformations are the same everywhere as the tip is scanned over the surface, the measured topography will be the same as if the substrate is rigid

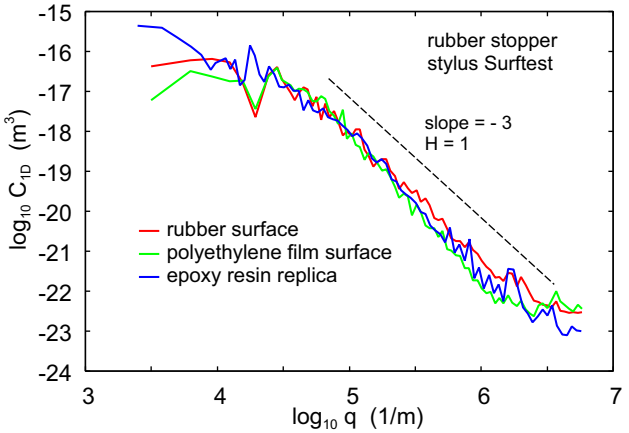

Fig. 24 The surface roughness topography of a rubber stopper used in a syringe. One part of the stopper is covered by a ∼ 10 μm thick polyethylene film, but the roughness on the rubber part (red curve) is nearly the same as on the polyethylene film (green curve). This shows that the roughness on both surfaces results from the steel mold. A replica of the stopper surface made from an elastically stiff epoxy resin has the same surface roughness power spectrum (blue curve) as the other two surfaces. This shows that tip-induced elastic deformation of the rubber surface has a negligible influence on the measured topography (see Fig. 23)

we have measured the surface topography of a soft (unfilled) rubber compound.

Figure 24 shows the surface roughness topography of a rubber stopper used in a syringe. The stopper was produced by injection molding with one part of the surface covered by a thin (∼ 10 μm thick) polyethylene film. The roughness on the rubber part (red curve) is nearly the same as on the polyethylene film (green curve) which indicates that the roughness on both surfaces results from the steel mold. A replica of the stopper surface made from an elastically stiff epoxy resin has the same power spectrum (replica of the rubber part, blue curve) as the other two surfaces. This shows that tip-induced elastic deformations of the rubber surface have a negligible influence on the measured topography.

A similar method was employed in the study referenced in [24], where the topography of smooth glass and silicone rubber replicas were measured, revealing significant differences. The discrepancy was attributed to stick-slip phenomena, likely

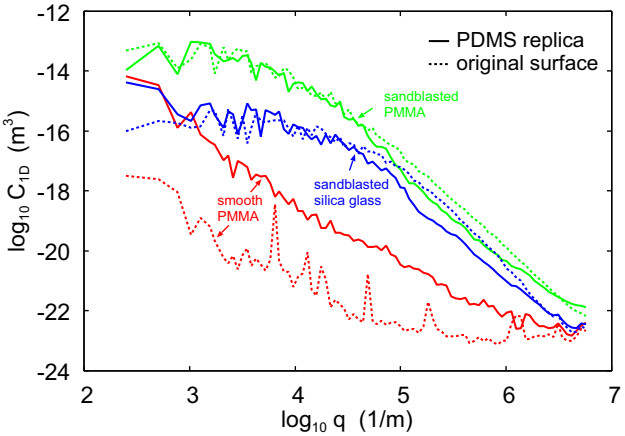

Fig. 25 The surface roughness power spectra of PDMS molded against three different surfaces, smooth PMMA (red), sandblasted silica glass (blue), and sandblasted PMMA (green). The solid lines are the power spectra of the PDMS replica and the dashed lines are of the originals. The power spectra were obtained using the Surftest stylus instrument by averaging over two line scans each 25 mm long

due to adhesion between the measurement tip and the silicone rubber. Compared to the current study, the rubber used for the stopper has an elastic modulus ∼ 1.5 times that of the silicone rubber, which is not significantly stiffer. Consequently, the difference in elastic modulus is unlikely to be the primary cause of the observed discrepancy. However, the silicone rubber replica in [24] was cast from a very smooth surface, unlike the rougher surface of the rubber stopper. It is known that sufficient surface roughness can eliminate macroscopic adhesion [46], where relevant roughness for this adhesion elimination corresponds to the roughness with a wavelength shorter than the width of the rubber-tip contact region, approximately 1 μm. We hypothesize that this is the main distinction between the two systems. To further substantiate this hypothesis, additional measurements were conducted on PDMS replicas of both smooth and sandblasted PMMA and silica glass surfaces.

Figure 25 shows the surface roughness power spectra of PDMS molded against three different surfaces, namely smooth PMMA (red), sandblasted silica glass (blue), and sandblasted PMMA (green). The power spectra were obtained using the Surftest stylus instrument by averaging over two line scans each 25 mm long. The solid lines are the power spectra of the PDMS replica and the dashed lines are of the originals. For the two sandblasted surfaces the PDMS replicas and the original surfaces give very similar power spectra, and in particular, the power spectra of the long wavelength roughness are well reproduced. This is also illustrated in Fig. 26 which shows the good agreement in height probability distribution of the sandblasted silica glass and PMMA surfaces (green lines) and the corresponding PDMS replicas (blue).

It can be observed that the power spectra of the smooth PMMA surface and its PDMS replica differ by several orders

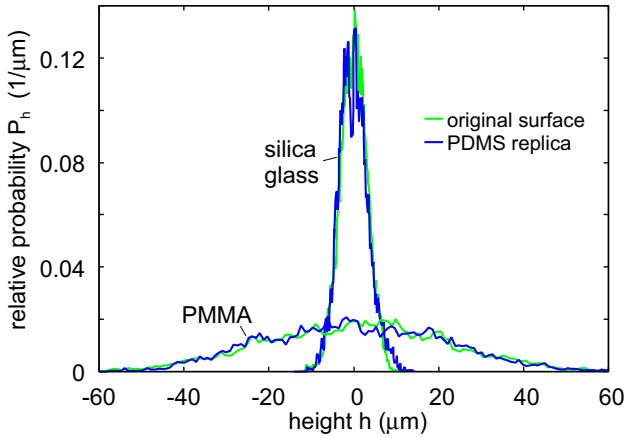

Fig. 26 The height probability distribution of the sandblasted silica glass and PMMA surfaces (green lines) and corresponding PDMS replicas (blue)

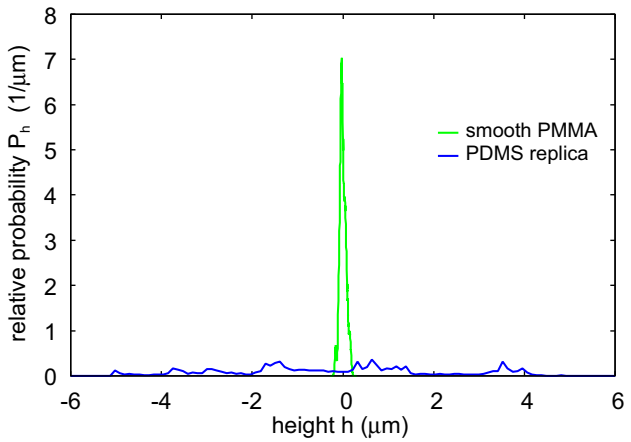

Fig. 27 The height probability distribution of the smooth PMMA surface (green line) and the PDMS replica of this surface (blue)

of magnitude. Additionally, the obtained height distributions are entirely different (see Fig. 27). This indicates that using engineering stylus measurements on soft rubbers with very smooth surfaces is likely to be unsuccessful. However, on surfaces with sufficient roughness, the stylus topography of the PDMS replica may be accurate. Nevertheless, considering our previous results for similar PDMS surfaces, there is no certainty that this will always be the case [24].

9 Discussion

We have compared the power spectra obtained from surface topography measurements using different experimental instruments. We found that stylus instruments (AFM and two engineering stylus) give overlapping power

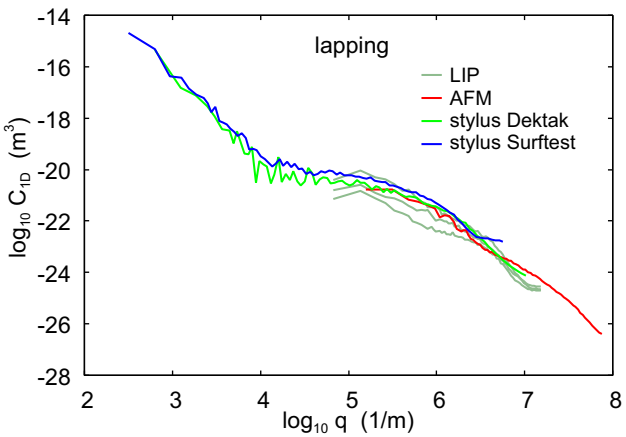

Fig. 28 The power spectrum of a lapped nickel surface (arithmetic average Ra = 0.05 μm) (FLEXBAR Model No. 16008, Surface Roughness Standards Set 800-879-7575)

spectra in the range of roughness length scales common to both techniques. The large modulus of the studied samples, the small tip diameter (8 nm for the AFM method), and the low contact forces applied in these two techniques result in accurate topography profiles and power spectra. For the surfaces studied, the power spectra obtained using optical instruments differed significantly from the results of the AFM and stylus studies. This is consistent with our earlier observations [47].

We note, however, that for other types of materials and other types of roughness, the optical methods may give useful results. This is illustrated in Fig. 28 where we compare stylus and AFM data with the optical LIP method for a lapped nickel surface used as a roughness standard.

Studies based on optical methods are fast and give nice-looking topography pictures, but our study shows that in general the relative size of surface structures cannot be trusted. We recommend against using optical methods for quantitative surface roughness studies.

10 Summary and Conclusion

Analytical contact mechanics theories depend on the surface roughness via the surface roughness power spectrum. We have shown that height data obtained using optical methods are often inaccurate and should not be used for calculating surface roughness power spectra, while engineering stylus instruments and atomic force microscopy (AFM) generally give good results. For surfaces with isotropic roughness, all information about the roughness is contained in a line scan if it is long enough. For this case, we have shown how the 2D

power spectrum $C_{2D}(q)$ can be obtained from the 1D power spectrum $C_{1D}(q)$ using different methods.

Appendix A: Power Spectra with Roll-Off Region

We assume that for both the 1D and 2D power spectra there is a flat roll-off region for $q_0 < q < q_r$ and (self affine fractal) power-law behavior for $q_r < q < q_1$. We denote a roll-off region as flat when the power spectrum is constant. We assume $q_0/q_r << 1$ and $q_r/q_1 << 1$ and $H > 0$. For this case if the 2D power spectrum

$$C_{2D} = C_0\left(\frac{q}{q_r}\right)^{-2(1+H)} \tag{A1}$$

for $q > q_r$ and

$$C_{2D} = C_0 \tag{A2}$$

for $q < q_r$ then (10) gives

$$h_{rms}^2 = 2\pi C_0 \int_{q_r}^{\infty} dkk \left(\frac{k}{q_r}\right)^{-2(1+H)} + 2\pi C_0 \int_0^{q_r} dkk$$

giving

$$C_0 = \frac{1}{\pi} h_{rms}^2 \frac{H}{1+H}\frac{1}{q_r^2}$$

In a similar way to the 1D power spectrum one can show that for $q_r < q$

$$C_{1D} = \frac{1+H}{1+2H}\pi q_r C_0\left(\frac{q}{q_r}\right)^{-1-2H} \tag{A3}$$

and for $q < q_r$

$$C_{1D} = \frac{1+H}{1+2H}\pi q_r C_0 \tag{A4}$$

so C_{1D} is continuous for $q = q_r$.

Suppose we know that C_{1D} is of the form (A3)-(A4). In this case, if the 2D power spectrum is of the form (A1)-(A2), then in the self-affine fractal region $C_{2D} = \pi q C_{1D}(1+2H)/(1+H)$. This relation is not valid in the roll-off region and is not exact even for $q > q_r$ as we will show below. This implies that if the 1D power spectrum has a flat roll-off region, this is not the case for the corresponding 2D power spectrum.

Assume that the 1D power spectrum is given by (A3)-(A4). Substituting (A3) in (13) and writing $k = xq_r$ gives for $q > q_r$ the 2D power spectrum

$$C_{2D} = C_0(1+H)\left(\frac{q}{q_r}\right)^{-2(1+H)} \int_1^{\infty} dx \frac{x^{-2-2H}}{(x^2-1)^{1/2}} \tag{A5}$$

and for $q < q_r$ we get

$$C_{2D} = C_0(1+H)\int_1^{\infty} dx \frac{x^{-2-2H}}{(x^2-(q/q_r)^2)^{1/2}} \tag{A6}$$

For $q/q_r << 1$ this gives

$$C_{2D} = C_0(1+H)\int_1^{\infty} dx\, x^{-3-2H} = \frac{1}{2}C_0$$

For $q > q_r$ we write

$$C_{2D} = C_0\left(\frac{q}{q_r}\right)^{-2-2H} g_2(H), \tag{A7}$$

where

$$g_2(H) = (1+H)\int_1^{\infty} dx \frac{x^{-2-2H}}{(x^2-1)^{1/2}} \tag{A8}$$

In Fig. 29 we show $g_2(H)$.

The analysis above shows that if C_{1D} has a self-affine region and a flat roll-off region then C_{2D} will have a self-affine region which differs by a constant factor $g_2(H)$ from what one would expect if the roll-off region of C_{2D} would be flat [compare (A1) with (A7)]. Indeed the roll-off region close to q_r [as given by (A6)] is not perfectly flat as shown in Fig. 30. We note that the exact form of the roll-off region is usually not very important and for most purposes the 2D power spectrum can be obtained from (A7) with q_r, h_{rms} and H determined from the 1D power spectrum. This is equivalent to using the relation

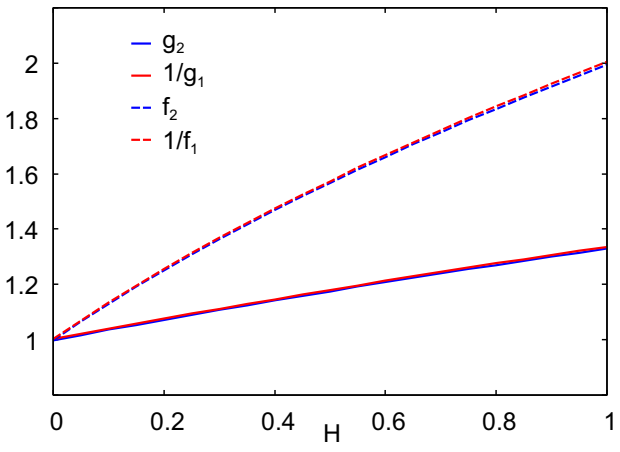

Fig. 29 The 2D power spectrum factors $g_2(H)$ and $f_2(H)$, and the inverse $1/g_1(H)$ and $1/f_1(H)$ of the 1D power spectrum factors, as a function of the Hurst exponent H

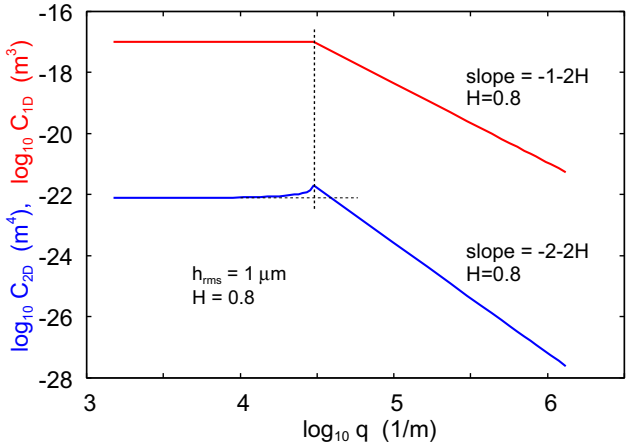

Fig. 30 The 1D (red line) and 2D (blue line) power spectra for a randomly rough surface with the rms roughness $h_{\rm rms} = 1$ μm and Hurst exponent $H = 0.8$. The 1D power spectrum has a flat roll-off region and the 2D power spectrum is calculated from C_{1D} using (13). The small, large and roll-off wavenumbers are $q_0 = 1 \times 10^3$ m^{-1}, $q_1 = 2048 \times 10^3$ m^{-1} and $q_r = 30 \times 10^3$ m^{-1}, respectively

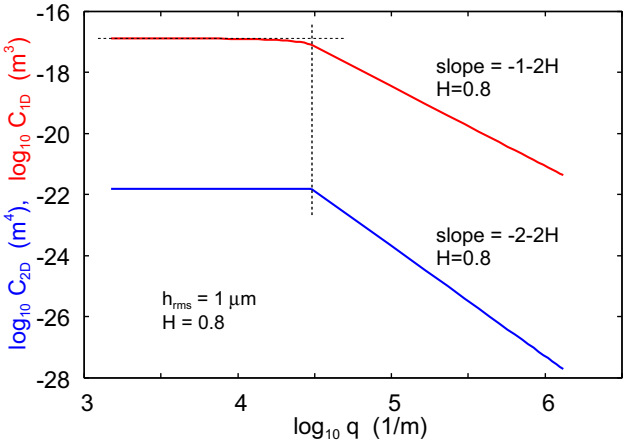

Fig. 31 The 1D (red line) and 2D (blue line) power spectra for a randomly rough surface with the rms roughness $h_{\rm rms} = 1$ μm and Hurst exponent $H = 0.8$. The 2D power spectrum has a flat roll-off region and the 1D power spectrum is calculated from C_{1D} using (14). The small, large and roll-off wavenumbers are $q_0 = 1 \times 10^3$ m^{-1}, $q_1 = 2048 \times 10^3$ m^{-1} and $q_r = 30 \times 10^3$ m^{-1}, respectively

$C_{2D} = f_2(H)C_{1D}/(\pi q)$ with $f_2(H) = g_2(H)(1+2H)/(1+H)$ and a constant in the roll-off region given by $C_{2D}(q_r)$.

In Sec. 3 we studied the power spectrum of a rough surface which was generated using the power spectrum with a 2D power spectrum with a flat roll-off. In this case, the 1D power spectrum does not have a perfectly flat roll-off region but instead shows a region close to q_r with reduced magnitude (see Fig. 2). This result also follows from the related relation (14) as we now will show.

Assume that the 2D power spectrum is given by (A1)-(A2). Using (A1) and (A2) in (14) and writing $k = xq_r$ gives for $q > q_r$ the 1D power spectrum

$$C_{1D} = 2C^0 q_r \left(\frac{q}{q_r}\right)^{-1-2H} \int_1^\infty dx \, \frac{x^{-1-2H}}{(x^2-1)^{1/2}} \tag{A9}$$

and for $q < q_r$ we get

$$C_{1D} = 2C^0 \left[\left(q_r^2 - q^2\right)^{1/2} + q_r \int_1^\infty dx \, \frac{x^{-1-2H}}{(x^2 - (q/q_r)^2)^{1/2}}\right] \tag{A10}$$

For $q/q_r << 1$ this gives

$$C_{1D} = \frac{4}{\pi}\frac{1+H}{1+2H}\pi q_r C_0 \tag{A11}$$

The analysis above shows that if C_{2D} has a self-affine region and a flat roll-off region then C_{1D} will have a self-affine region that differs by a constant factor $g_1(H)$ from what one would expect if the roll-off region of C_{1D} would be flat [compare (A3) with (A11)]. Indeed the roll-off region close to q_r [as given by (A11)] is not perfectly flat as shown in Fig. 31.

For $q > q_r$ we write

$$C_{1D} = \frac{1+H}{1+2H}\pi q_r C_0 \left(\frac{q}{q_r}\right)^{-1-2H} g_1(H), \tag{A12}$$

where

$$g_1 = \frac{2}{\pi}\frac{1+2H}{1+H}\int_1^\infty dx \, \frac{x^{-1-2H}}{(x^2-1)^{1/2}} \tag{A13}$$

We write $C_{1D} = f_1(H)\pi q C_{2D}$ with $f_1(H) = g_1(H)(1+H)/(1+2H)$ and a constant in the roll-off region given by $C_{1D}(q_r)$. In Fig. 29 we show $1/g_1(H)$ and $1/f_1(H)$. Note that $1/g_1 \approx g_2$ and $1/f_1 \approx f_2 \approx (1+3H)^{1/2}$ Hence we can use the relation $C_{2D} = f(H)C_{1D}/(\pi q)$ with $f(H) \approx (1+3H)^{1/2}$ to calculate C_{2D} in the self-affine fractal region when C_{1D} is given (with a flat roll-off region), and also to calculate C_{1D} in the self-affine fractal region when C_{2D} is given (with a flat roll-off region). In practical applications only the first application is relevant.

Acknowledgements We thanks Professor Nicholas Strandwitz and his group from LeHeigh University, Allentown, USA for the XRR measurements. We thank T.D.B. Jacobs, N. Miller, M.H. Müser and L. Pastewka for the samples used for the topography study. We thank Cynthia Fuentes (BD Medical, Le Pont de Claix, France) and Mike Pena (BD Medical, Franklin Lakes, NJ, US) for help with optical and laser profilometry measurements, and Niko Cosa (Keyence, US) for help with white light profilometry and A.E. Yakini (MultiscaleConsulting and FZ Jülich) for performing the Mitutoyo stylus measurements, and Istiaque Choudhury and Nicholas Strandwitz (Materials Science and Engineering, at Lehigh University, Allentown, PA, US) for the XRR measurement and comments. This work was by the Strategic Priority Research Program of the Chinese Academy of Sciences, Grant No. XDB0470200. We acknowledge the contribution of Prof. Nicholas Strandwitz from Lehigh University, PA, USA, for performing the XRR measurements.

Funding Open Access funding enabled and organized by Projekt DEAL.

References

1. Jacobs, T.D.B., Pastewka, L.: Surface topography as a material parameter. MRS Bull **47**, 1205–1210 (2022)
2. Aghababaei, R., Brodsky, E.E., Molinari, J.F., Chandrasekar, S.: How roughness emerges on natural and engineered surfaces. MRS Bull. **47**, 1229–1236 (2022)
3. Persson, B.N.J.: Functional properties of rough surfaces from an analytical theory of mechanical contact. MRS Bull. **47**, 1211–1219 (2022)
4. Müser, M.H., Nicola, L.: Modeling the surface topography dependence of friction, adhesion, and contact compliance. MRS Bull. **47**, 1221–1228 (2022)
5. Weber, B., Scheibert, J., de Boer, M.P., Dhinojwala, A.: Experimental insights into adhesion and friction between nominally dry rough surfaces. MRS Bull. **47**, 1237–1246 (2022)
6. Wieland, M., Textor, M., Spencer, N.D., Brunette, D.: Wavelength-dependent roughness: a quantitative approach to characterizing the topography of rough titanium surfaces. Int. J. Oral Maxillofac. Implants **16**, 163 (2001)
7. Persson, B.N.J., Gorb, S.: The effect of surface roughness on the adhesion of elastic plates with application to biological systems. J. Chem. Phys. **119**, 11437 (2003)
8. Dai, Z., Gorb, S.N., Schwarz, U.: Roughness-dependent friction force of the tarsal claw system in the beetle *Pachnoda marginata* (Coleoptera, Scarabaeidae). J. Exp. Biol. **205**, 2479 (2002)
9. Persson, B.N.J.: On the mechanism of adhesion in biological systems. J. Chem. Phys. **118**, 7614 (2003)
10. Majhy, B., Priyadarshini, P., Sen, A.K.: Effect of surface energy and roughness on cell adhesion and growth-facile surface modification for enhanced cell culture. RSC Adv. **11**, 15467 (2021)
11. Nayak, P.R.: Random process model of rough surfaces. ASME J. Lubr. Technol. **93**, 398 (1971)
12. Persson, B.N.J.: On the use of surface roughness parameters. Tribol. Lett. **71**, 29 (2023)
13. Pawar, G., Pawlus, P., Etsion, I.: The effect of determining topography parameters on analyzing elastic contact between isotropic rough surfaces. J. Tribol. **135**, 011401 (2013)
14. Persson, B.N.J., Albohr, O., Tartaglino, U., Volokitin, A.I., Tosatti, E.: On the nature of surface roughness with application to contact mechanics, sealing, rubber friction and adhesion. J. Phys. **17**, R1 (2004)
15. Persson, B.N.J.: On the fractal dimension of rough surfaces. Tribol. Lett. **54**, 99 (2014)
16. Jacobs, T.D.B., Junge, T., Pastewka, L.: Quantitative characterization of surface topography using spectral analysis. Surf. Topogr. Metrol. Prop. **5**, 013001 (2017)
17. Persson, B.N.J.: Theory of rubber friction and contact mechanics. J. Chem. Phys. **115**, 3840 (2001)
18. Almqvist, A., Campana, C., Prodanov, N., Persson, B.N.J.: Interfacial separation between elastic solids with randomly rough surfaces: comparison between theory and numerical techniques. J. Mech. Phys. Solids **59**, 2355 (2012)
19. Afferrante, L., Bottiglione, F., Putignano, C., Persson, B.N.J., Carbone, G.: Elastic contact mechanics of randomly rough surfaces: an assessment of advanced asperity models and Persson's theory. Tribol. Lett. **66**, 1 (2018)
20. Longuet-Higgins, M.S.: The statistical analysis of a random. Moving surface. Philos. Trans. Roy. Sot. **A249**, 321 (1957)
21. Longuet-Higgins, M.S.: The statistical geometry of random surfaces. Hydrodynamic stability. In: Proceedings of 13th Symposia in Applied Mathematics. American Mathematical Society, Providence (1962)
22. Whitehouse, D.J., Archard, J.F.: The properties of random surfaces of significance in their contact. Proc. R. Soc. (Lond.) **316**, 97 (1970)
23. Gray, G.G., Johnson, K.L.: The dynamic response of elastic bodies in rolling contact to random roughness of their surfaces. J. Sound Vib. **22**, 323 (1972)
24. Persson, J.S., Tiwari, A., Valbahs, E., Tolpekina, T.V., Persson, B.N.J.: On the use of silicon rubber replica for surface topography studies. Tribol. Lett. **66**, 140 (2018)
25. Lahayne, O., Pichler, B., Reihsner, R., Eberhardsteiner, J., Suh, J., Kim, D., Nam, S., Paek, H., Lorenz, B., Persson, B.N.J.: Rubber friction on ice: experiments and modeling. Tribol. Lett. **62**, 17 (2016)
26. Wang, C., Lv, D., Shi, H., Liu, X., Xin, R.: Discussion on method of optical surface roughness measurement. In: Zhang, C., Asundi, A. (eds.) Second International Conference on Photonics and Optical Engineering. Proceedings of SPIE, vol. 10256, p. 1025654 (2017). SPIE
27. Cunningham, T., Serry, F.M., Ge, L.M., Dawson, D.J.: Atomic force profilometry and long scan atomic force microscopy: new techniques for characterisation of surfaces. Surf. Eng. **16**, 295–298 (2000)
28. Gujrati, A., Khanal, S.R., Pastewka, L.: TDB Jacobs Combining TEM, AFM, and profilometry for quantitative topography characterization across all scales. ACS Appl. Mater. Interfaces **10**, 29169 (2018)
29. Sinha, S.K.: Surface roughness by X-ray and neutron scattering methods. Acta Phys. Pol. A **89**, 219 (1996)
30. Klingaa, C.G., Zanini, F., Mohanty, S., Carmignato, S., Hattel, J.H.: Characterization of geometry and surface texture of AlSi10Mg laser powder bed fusion channels using X-ray computed tomography. Appl. Sci. **11**, 4304 (2021)
31. Wiesendanger, R.: Scanning Probe Microscopy and Spectroscopy. Cambridge University Press, Cambridge (1994)
32. Church, E.L., Takacs, P.Z.: Effects of the nonvanishing tip size in mechanical profile measurements. In: Proceeding of the SPIE 1332, Optical Testing and Metrology III: Recent Advances in Optical Inspection (1991). https://doi.org/10.1117/12.51099
33. Knoll, A.W.: Nanoscale contact-radius determination by spectral analysis of polymer roughness images. Langmuir **29**, 13958 (2013)
34. Persson, B.N.J.: Adhesion between an elastic body and a randomly rough hard surface. Eur. Phys. J. E **8**, 385 (2002)
35. Carbone, G., Lorenz, B., Persson, B.N.J., Wohlers, A.: Contact mechanics and rubber friction for randomly rough surfaces with anisotropic statistical properties. Eur. Phys. J. E **29**, 275 (2009)

36. Jacobs, T.D.B., Miller, N., Müser, M.H., Pastewka, L.: The surface-topography challenge: problem definition. https://arxiv.org/abs/2206.13384
37. Rayleigh, L.: Theory of Sound, vol. II, pp. 80–96. Macmillian, London (1929)
38. Rice, S.O.: Reflection of electromagnetic waves from slightly rough surfaces. Commun. Pure Appl. Math. **4**, 351 (1951)
39. Barrick, D.E.: Radar Cross Section Handbook. Plenum, New York (1970). (**Chapter 9**)
40. Church, E.L., Jenkinson, H.A., Zavada, J.M.: Measurement of the finish of diamond turned metal surfaces by differential light scattering. Opt. Eng. **16**, 360 (1977)
41. Lederman, D., Yu, Z., Myers, T.H., Richards-Babb, M.R.: Surface morphology of GaN films determined from quantitative X-ray reflectivity. Appl. Phys. Lett. **71**, 368 (1997)
42. Persson, B.N.J.: Influence of surface roughness on press fits. Tribol. Lett. **71**, 19 (2023)
43. Gadelmawla, E.S., Koura, M.M., Maksoud, T.M.A., Elewa, I.M., Soliman, H.H.: Roughness parameters. J. Mater. Process. Technol. **123**, 133 (2002)
44. GAR: G-6 Microfinish Comparator Surface Finish Scale. Gar Electroforming Div. Electroformers, Danbury, CT, USA
45. Persson, B.N.J., Mate, C.M.: Role of humidity and surface roughness on direct wafer bonding. Eur. J. Phys. B **97**(4), 1–13 (2024)
46. Tiwari, A., Wang, J., Persson, B.N.J.: Adhesion paradox: why adhesion is usually not observed for macroscopic solids. Phys. Rev. E **102**, 042803 (2020)
47. Lorenz, B., Persson, B.N.J., Dieluweit, S., Tada, T.: Rubber friction: comparison of theory with experiment. Eur. Phys. J. E **34**, 129 (2011). Fig. 6 in this reference compare the power spectrum, obtained using a white light interferometry sensor and an infinite focus microscope, with the power spectra obtained from engineering stylus and AFM data